4

ELECTRON-NUCLEAR DOUBLE RESONANCE (ENDOR)

4.1. Introduction

In hydrated crystals such as many paramagnetic salts of the iron group, the magnetic ion is surrounded by a number of water molecules. The line width of the electron spin resonance spectrum, even in a highly diluted specimen at such low temperatures that the spin lattice relaxation time is too long to give an appreciable contribution, is of order 10 G, or about 30 MHz for $g = 2$. This line width is due mainly to the local magnetic fields of the proton nuclear moments in the water molecules. In a deuterated crystal this can be reduced by a factor of about $\frac{1}{3}$, because of the smaller nuclear magnetic moment of the deuteron. In oxides such as MgO, CaO, or ThO_2, where only a minority of the nuclei have magnetic moments, the line width may be about 1 G or smaller (dependent on crystal imperfections), corresponding to a few MHz in frequency units. This residual line width sets a limit to the accuracy with which measurements of the position of the line may be made, which in very round terms we may take to be of the order of 1 MHz.

In the determination of a hyperfine structure parameter from a spin resonance spectrum, measurements must be made of the positions of successive lines, and the parameter is deduced from the differences in these positions. When anisotropy is present, it is best to make measurements along each of the principal axes; not only does this give directly the 'diagonal' components of any 'tensor' interaction, but the positions of the spin resonance lines are then passing through extrema, and small inaccuracies in orientation of the external magnetic field are least important. The accuracy with which the magnetic hyperfine parameter A can be determined is then limited by the considerations of line width set out above. The other hyperfine parameters such as a nuclear electric quadrupole interaction or the nuclear Zeeman interaction with the external magnetic field are more difficult to determine because they are usually rather small, and their presence is revealed in the electron spin resonance spectrum only if the simple selection rule $\Delta m = 0$ is broken down. In many cases this means that measurements must be made with the external field at an angle to the principal axes

of the hyperfine 'tensor', in order that otherwise 'forbidden' lines can be observed. Even in cases where this is possible, the accuracy of such measurements is rather restricted, and the determination of signs of the parameters is, to say the least, awkward.

It is true that if measurements are made in zero or rather small magnetic field, transitions of the type $\Delta m \neq 0$ have matrix elements comparable with those for which $\Delta m = 0$ (cf. § 3.9 and Fig. 3.12), and have been observed, for example, by Bleaney, Scovil, and Trenam (1954). Such transitions have line widths comparable with those quoted above, and they generally occur in frequency regions where the sensitivity of a magnetic resonance spectrometer is inherently much lower, with the additional drawback of having to sweep over a wide frequency range.

The accuracy of such hyperfine measurements, and the total information content, would be greatly improved if nuclear transitions could be observed directly, particularly in strong external magnetic fields where the nuclear Zeeman interaction is not unduly small. Unfortunately the matrix elements for such transitions involve (in the strong field limit of complete decoupling) only the nuclear magnetic moment, and the transitions are correspondingly weak, though there is some enhancement in practice of the oscillatory field at the nuclear frequency (see below and § 4.3). In this chapter we describe a technique by which these problems are solved. In §§ 4.2–4.8 we shall be primarily concerned with hyperfine interactions with the nuclear moments of the paramagnetic ion itself; these are usually associated with a resolved hyperfine structure in the electron resonance spectrum, and the approximation $A \gg g_I\beta H$ is generally valid. They can also be applied to unresolved hyperfine structure due to ligand nuclei (the cause of the line widths mentioned above); the relevant hyperfine parameters are then usually comparable with $g_I\beta H$. This rather different case is discussed in more detail in § 4.9.

The difficulties are overcome by the method of Electron-Nuclear DOuble Resonance, or Endor, invented by Feher (1956*b*). The method has been outlined in § 1.13, and here we illustrate the principles briefly by reference to a system with $S = \frac{1}{2}$, $I = \frac{1}{2}$. In the absence of anisotropy, the spin Hamiltonian is

$$\mathscr{H} = g\beta(\mathbf{H} \cdot \mathbf{S}) + A(\mathbf{S} \cdot \mathbf{I}) - g_I\beta(\mathbf{H} \cdot \mathbf{I}). \tag{4.1}$$

In a strong magnetic field ($g\beta H \gg A \gg g_I\beta H$) the levels are approximately as shown in Fig. 4.1. The electronic states $M = +\frac{1}{2}$ lie above

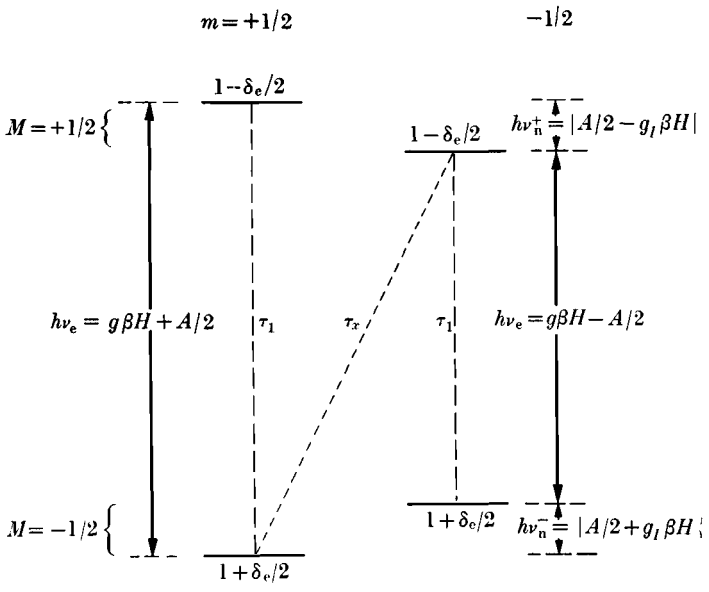

FIG. 4.1. The energy level scheme for $S = I = \frac{1}{2}$, showing the level populations in thermal equilibrium in the approximation where $\delta_e = (h\nu_e/kT) \ll 1$, and $\delta_n = (h\nu_n/kT)$ is neglected. The relaxation paths are indicated by broken lines, the vertical paths being the more rapid ($\tau_1 \ll \tau_x$); other, slower, relaxation paths are omitted.

the $M = -\frac{1}{2}$ states by about $g\beta H$, while the nuclear states with the same value of M are separated by $(\pm A/2 - g_I\beta H)$, if we ignore for the present terms of order $A^2/g\beta H$.

In thermal equilibrium the populations are approximately $1 \pm \delta_e/2$, where $\delta_e = (g\beta H/kT) = (h\nu_e/kT)$, provided that $\delta_e \ll 1$. Here $h\nu_e$ is the quantum required for electron magnetic resonance, and for the $\Delta m = 0$ transitions

$$h\nu_e = |g\beta H \pm A/2|, \tag{4.2}$$

but we ignore the correction to δ_e due to the term in A. This is equivalent to ignoring the small differences in population of order $\delta_n = (h\nu_n/kT)$, where $h\nu_n$ is the quantum required for a nuclear magnetic resonance transition, which is

$$\begin{aligned} h\nu_n^+ &= |+A/2 - g_I\beta H| \\ h\nu_n^- &= |-A/2 - g_I\beta H| \end{aligned} \tag{4.3}$$

for the $M = +\frac{1}{2}$, $m = +\frac{1}{2} \leftrightarrow -\frac{1}{2}$ and $M = -\frac{1}{2}$, $m = +\frac{1}{2} \leftrightarrow -\frac{1}{2}$ transitions respectively. The population differences are maintained by means of relaxation to the lattice through the paths marked by broken lines, the vertical paths being usually the more rapid in action.

If only a weak electron magnetic resonance driving field is applied to either of the $\Delta M = \pm 1$, $\Delta m = 0$ transitions, the populations will remain substantially unaltered; this is also true if we apply simultaneously a driving field at the nuclear magnetic resonance frequency, and since this does not appreciably affect the intensity of the electron magnetic resonance signal, the nuclear transition will remain undetected, being too weak to be observed directly. If, instead, a strong magnetic resonance driving field is applied to either of the $\Delta M = \pm 1$, $\Delta m = 0$ transitions, the difference between the populations of the two levels involved will be reduced and, in the limit of complete saturation, they will become equal. If the relaxation time for the sloping relaxation path is τ_x, the populations of the two $m = -\frac{1}{2}$ states will remain unaltered for a time short compared with τ_x if the $m = +\frac{1}{2}$ transition is saturated; and vice versa (see Fig. 4.2(a)). Thus we have a population

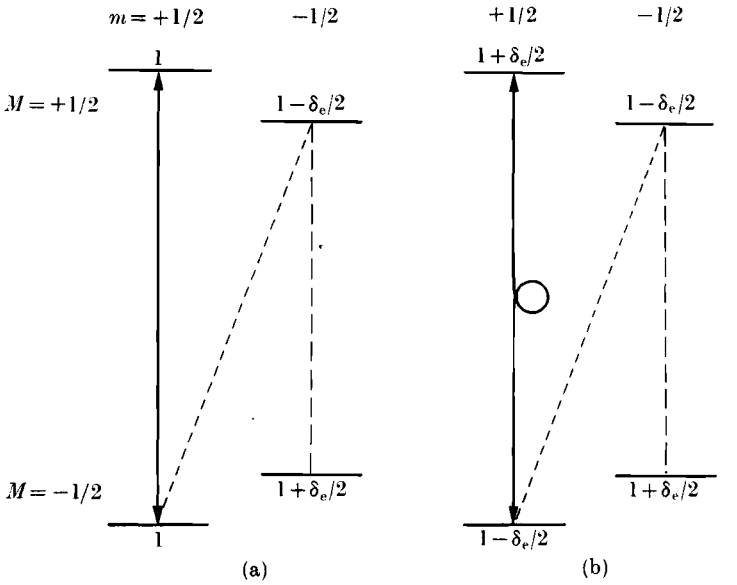

FIG. 4.2. The level populations in the system $S = I = \frac{1}{2}$, after (a) saturation of the electronic $(+\frac{1}{2}, +\frac{1}{2}) \leftrightarrow (-\frac{1}{2}, +\frac{1}{2})$ transition, (b) adiabatic rapid passage through the same transition, in each case before the populations of the $m = -\frac{1}{2}$ levels are affected through the sloping relaxation path. In (a) the populations of the two levels involved in the electronic magnetic resonance are equalized; in (b) the populations are inverted.

difference of order δ_e between adjacent nuclear levels $m = \pm\frac{1}{2}$ with the same value of M, where formerly the population difference was (in our approximation) zero. Under these conditions the effect of applying a nuclear magnetic resonance driving field to the $\Delta M = 0$,

$\Delta m = \pm 1$ transitions is enhanced, though not usually enough to make them directly detectable. However, if this driving field is strong enough to induce nuclear transitions at a rate faster than $1/\tau_x$, the population of the two $m = +\frac{1}{2}$ levels will be appreciably altered, with a resultant change in the intensity of the electron magnetic resonance absorption between these two levels. Obviously the effect is greatest when the nuclear driving field is at either of the resonant values given by eqn (4.3), so that we have a method of determining these two frequencies (and hence measuring A and $g_I\beta H$) through the effect on the electron paramagnetic resonance signal, with a sensitivity comparable with that in a simple electron paramagnetic resonance experiment.

When the relaxation times are exceptionally long, as in the original experiments of Feher on donors in silicon, it may be more convenient to use the technique of adiabatic rapid passage. This results in inversion, instead of equalization, of the populations of the two levels involved, as shown in Fig. 4.2(b). Clearly the situation as regards the difference in population between adjacent nuclear levels resembles that in Fig. 4.2(a) (actually the differences are twice as large), so that application of the appropriate nuclear resonance frequency will again affect the intensity of the electron resonance signal, as measured either by application of a weak driving field at the electron resonance frequency, or by a further traverse of the electronic line under adiabatic rapid passage conditions.

The major advance in an Endor type experiment is that, not only does it enable us to measure the hyperfine interaction constants and the nuclear Zeeman interaction directly, but it also gives them with much higher precision. In fact much greater (fractional) precision may be obtained in the measurement of A in an Endor experiment than of g in a simple electron paramagnetic resonance experiment. As indicated in § 1.13, this is possible only when we are dealing with inhomogeneously broadened lines. We shall not at this point repeat the reasons for the high precision obtainable when this requirement is satisfied (see § 1.13), believing that the experimental results reported later in this chapter will serve as an adequate demonstration. Essentially it stems from the fact that the nuclear resonance is taking place in the electronic field H_e (see § 1.2), which is of order 10^5 to 10^6 G, rather than just the applied field H, but the line width may still be only a few gauss.

This large electronic field also assists in enhancing the nuclear transition rate w_n. As indicated above, this rate must be at least comparable with $1/\tau_x$ in order to affect the level populations sufficiently

to produce an observable change in intensity in the electron paramagnetic resonance signal. For a nucleus with $g_I \sim 10^{-3}$, and an r.f. field amplitude $H_1 = 1$ G, we have $w_n \sim 10^3\ s^{-1}$ if the Endor line width is 10 kHz, and $10^2\ s^{-1}$ if it is 100 kHz; this is sufficient only if τ_x is greater than 10^{-3} or 10^{-2} s respectively, so that any enhancement in w_n may be very important. The enhancement produced by the electronic field H_e at the nucleus may be understood classically from Fig. 4.3.

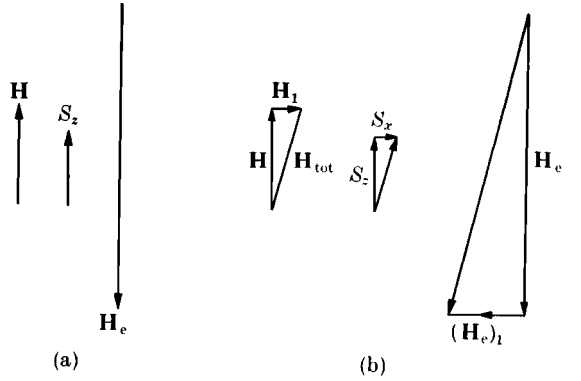

FIG. 4.3. (a) Direction of a steady magnetic field **H** along the z-axis, the component S_z of the electron spin, and the electronic field at the nucleus $\mathbf{H}_e = -(AS_z/g_I\beta)$; (b) when a low-frequency oscillatory field $\mathbf{H}_1$ is applied normal to **H**, both the electron spin and the electronic field $\mathbf{H}_e$ follow the resultant external field $\mathbf{H}_{tot}$, setting up an additional oscillatory field $(\mathbf{H}_e)_1$ at the nucleus, which is larger than $\mathbf{H}_1$ by a factor $|(H_e/H)|$.

Suppose the steady external field **H** is applied in the z-direction; then, assuming no anisotropy, the electronic magnetic moment corresponding to a given value of S_z is also directed along the z-axis, and this sets up an electronic field $\mathbf{H}_e$ at the nucleus, corresponding to the term $AS_zI_z = -g_I\beta H_eI_z$, which is also along the z-axis, but oppositely directed to S_z if (A/g_I) is positive. The application of an oscillatory field $\mathbf{H}_1$ normal to the z-axis gives a resultant field $\mathbf{H}_{tot}$ inclined at an angle $\theta \sim (H_1/H)$ (assumed small) to the z-axis. If $\mathbf{H}_1$ is a rotating field, then $\mathbf{H}_{tot}$ rotates about the z-axis; if $\mathbf{H}_1$ is a linearly polarized field along (say) the x-axis, then $\mathbf{H}_{tot}$ oscillates about the z-axis in the zx-plane. Provided that $\mathbf{H}_1$ oscillates at a frequency low compared with the electronic Larmor frequency (see § 2.4), the direction of the electronic magnetization will follow $\mathbf{H}_{tot}$, setting up an oscillatory field $(\mathbf{H}_e)_1$ at the nucleus, as in Fig. 4.3(b). Although $(\mathbf{H}_e)_1$ is here oppositely directed to $\mathbf{H}_1$, it is of order $\theta H_e = (H_1/H)H_e = H_1(H_e/H)$, and so may be as much as 100 times or more larger than the externally applied field

H_1. As can be seen, the degree of enhancement is proportional to H_e and hence to $S_z = M$, and thus is largest for the largest values of $|M|$, vanishing for $M = 0$.

This enhancement process is simply a form of 'paramagnetic anti-shielding' (equivalent to an enormous 'chemical shift'), and is similar to that which occurs *within* a domain in a ferromagnetic substance. In a paramagnetic substance the situation may be complicated through the presence of anisotropy. A quantum-mechanical analysis is given in § 4.3.

In the following section (§ 4.2) we carry out a somewhat tedious but necessary analysis of the information that can be obtained from Endor measurements. Also, § 4.3 contains a rather detailed analysis of the enhancement of the nuclear transition probability, and the reader who wishes to obtain a general picture of the power of the Endor method may prefer to read first the outline of the elegant experiments of Feher, given in §§ 4.4 and 4.5.

4.2. The Endor spectrum

In general, the accuracy of Endor measurements is such that they must be fitted to a numerical solution of the spin Hamiltonian evaluated by means of a computer—approximate methods of solution using perturbation theory will not suffice. However, to discover what information can be obtained from the Endor spectrum it is convenient to make use of the formulae obtained in the previous chapter for the energy levels, using perturbation theory. An important question is—what information do the experiments give about the signs of the parameters in the spin Hamiltonian, as well as their numerical magnitudes. To simplify this problem we shall use the approximate formulae derived in the last chapter for the energy levels in a strong magnetic field with arbitrary orientation. As before, we assume that quantities such as $G = g\beta H$, A are necessarily positive, though the principal values of the $\mathbf{g}$ and $\mathbf{A}$ 'tensors' may be of either sign. As a further simplification, we consider first the case of an ion with effective spin $S = \frac{1}{2}$ and magnetic hyperfine structure only.

$S = \frac{1}{2}$, magnetic hyperfine structure only, axial symmetry

A typical Endor transition is that in which the nuclear magnetic quantum number changes by one unit while the electronic quantum number remains fixed. We shall therefore consider always the transition $|M, m\rangle \leftrightarrow |M, m-1\rangle$. From the formula for the energy levels given in

eqn (3.54), this requires a quantum of energy

$$|h\nu_n| = AM-(A_{\parallel}A_{\perp}^2/4AG)-G_I- \\ -M(2m-1)\left\{(A_{\parallel}^2+A^2)(A_{\perp}^2/4A^2G)+\frac{(A_{\parallel}^2-A_{\perp}^2)^2}{8A^2G}\left(\frac{g_{\parallel}g_{\perp}}{g^2}\right)^2\sin^2 2\theta\right\}. \quad (4.4)$$

This formula applies to the case where **H** is applied at an angle θ to the unique axis of an ion with axial symmetry, so that $G = g\beta H$ where g is defined by eqn (3.14), and A is defined by eqn (3.51). G_I is the diagonal part of the nuclear Zeeman term as defined by eqn (3.55), so that we are making the implicit assumption that $A \gg G_I$. If linearly polarized radiation is used to induce the nuclear Endor transition, we cannot tell experimentally which of the two levels involved is the higher and we therefore write $h\nu_n$ within modulus signs.

The terms contained in eqn (4.4) are of three types:

(i) AM, which has the values $+A/2$ or $-A/2$ according to the electronic energy level involved. Since the Endor transition is detected by the change in the intensity of the electronic transition $M \leftrightarrow M-1$, transitions in both the levels $M = +\frac{1}{2}$ and $-\frac{1}{2}$ will in general be observed while sitting on a given hyperfine line in the e.s.r. spectrum (see § 4.6);

(ii) the two terms $(A_{\parallel}A_{\perp}^2/4AG)+G_I$, which occur together and are independent of M and m. These two terms can be separated by measurements at different e.s.r. frequencies (different magnetic fields), since the term with G in the denominator varies as H^{-1} while G_I varies as H. To obtain good accuracy in measuring the two terms separately it is preferable to make measurements at widely different fields, but it may also be possible to calculate the first term with sufficient accuracy from the known values of the hyperfine parameters and g.

(iii) the last term, which involves both M and m in the form $M(2m-1)$. This term vanishes for $m = \frac{1}{2}$, and otherwise may be calculable with sufficient accuracy, as in (ii).

The different dependences on M and on m mean that by making sufficient measurements all three terms can be evaluated separately, while the two terms in (ii) can be separated using measurements at different electron resonance frequencies. This raises the general question, how many different measurements can be made? Clearly this number can be multiplied by making Endor measurements over a range of different electron resonance frequencies, and to define the position we restrict ourselves to just one such frequency.

In practice, the Endor transitions $|M, m\rangle \leftrightarrow |M, m\pm 1\rangle$ and $|M-1, m\rangle \leftrightarrow |M-1, m\pm 1\rangle$ can usually be detected while observing just the one electronic hyperfine line $|M, m\rangle \leftrightarrow |M-1, m\rangle$. This means that at a single value of H, four Endor frequencies can be measured except for the hyperfine lines $m = \pm I$, for each of which obviously only two are possible. Altogether, for an ion with effective spin S the number of Endor frequency measurements possible is $16IS$, and this usually means that the hyperfine parameters are overdetermined, giving a valuable check on internal consistency.

We consider now the question of the determination of signs. Since we can measure only $|h\nu_n|$, only $|(A_\parallel A_\perp^2/4AG)+G_I|$ can be found, but as pointed out above these two terms can be measured separately by observations at different field strengths. Their relative sign is also determined in this process, and since we take A, G to be positive quantities, we know the sign of G_I relative to $A_\parallel$. However, from eqn (3.55),

$$gAG_I = \beta H(g_\parallel^{(I)} g_\parallel A_\parallel \cos^2\theta + g_\perp^{(I)} g_\perp A_\perp \sin^2\theta),$$

so that if we measure in the direction $\theta = 0$ we find, relative to $A_\parallel$, the sign of $g_\parallel^{(I)} g_\parallel A_\parallel$, and the final result is a determination of the sign of $g_\parallel^{(I)}$ relative to that of $g_\parallel$. This is the same result as is obtained by observation of the 'forbidden' lines in the electron spin resonance spectrum itself, as outlined in § 3.8. Measurement at $\theta = 90°$ would give the sign of G_I (i.e. of $g_\perp^{(I)} g_\perp A_\perp$) relative to that of $A_\parallel$, but as the signs of $g_\perp$ and $A_\perp$ are indeterminate, no fresh information is obtained.

It is possible, of course, to use circularly polarized radiation for the Endor transitions. If the largest term in eqn (4.4) is AM, we would need right-handed polarization for the transitions $m \leftrightarrow m-1$ in the electronic level $M = +\frac{1}{2}$, and left-handed polarization for those in $M = -\frac{1}{2}$. For simplicity, we consider just the transitions $m = +\frac{1}{2}$ to $-\frac{1}{2}$. If those requiring right-handed polarization have the higher frequency, then $G_I+(A_\parallel A_\perp^2/4AG)$ is negative (and vice versa), so that we find the sign of $A_\parallel$ unambiguously, together with that of the product $(g_\parallel^{(I)} g_\parallel)$, but the latter still gives the sign of $g_\parallel^{(I)}$ only relative to that of $g_\parallel$.

$S = \frac{1}{2}$, axial symmetry, including electric quadrupole interaction

We now include a term $P_\parallel\{I_z^2 - \frac{1}{3}I(I+1)\}$, which means that for an arbitrary orientation of the external magnetic field we must add to the energy in first order (i.e. if $P \ll A$) an amount

$$P\{m^2 - \tfrac{1}{3}I(I+1)\}, \tag{3.62}$$

where P is given by the equation

$$P = \tfrac{1}{2}P_{\parallel}\left(3\frac{g_{\parallel}^2 A_{\parallel}^2}{g^2 A^2}\cos^2\theta - 1\right).$$

There are also second-order terms in m/M and m^3/M, whose coefficients involve only the squares of $g_{\parallel}$, $g_{\perp}$, $A_{\parallel}$, $A_{\perp}$ and are therefore fixed in sign; these terms are given in eqn (3.63). In an Endor transition for $S = \frac{1}{2}$ these give rise to terms that behave like M, Mm, and Mm^2, which can all be sorted out by their angular dependence and give no further information. They vanish if measurements are made with the magnetic field along the unique axis, and considerable complications are thus avoided.

Essentially therefore we have to add to $|h\nu_n|$ for the transition $m \leftrightarrow m-1$ an increment $P(2m-1)$. In its dependence on m alone it differs from any of the terms in eqn (4.4) and it can therefore be evaluated separately by making sufficient measurements of different hyperfine lines. Since A is positive, the e.s.r. lines for positive m come at the low-field end of the spectrum for constant frequency (and vice versa). If we take the mean of the Endor transitions for a given value of m (i.e., the mean of the measurements for $M = +\frac{1}{2}$ and $-\frac{1}{2}$), we obtain the quantity

$$|P(2m-1) - G_I - (A_{\parallel}A_{\perp}^2/4AG)|,$$

and since we know the sign of m, we can determine the sign of P relative to those of $A_{\parallel}$ and G_I. But the sign of G_I can be found relative to that of $A_{\parallel}$, as already shown, so that we can find the sign of P (and hence of $P_{\parallel}$) relative to that of $A_{\parallel}$.

The conclusions we have reached about signs for the case of $S = \frac{1}{2}$ agree with those stated by Halford (1962), and can be summarized as follows:

(i) Endor gives the sign of $g_{\parallel}^{(I)}$ relative to that of $g_{\parallel}$;

(ii) Endor gives the sign of $P_{\parallel}$ relative to that of $A_{\parallel}$.

In addition, if circularly polarized nuclear radiation is used,

(iii) the sign of $A_{\parallel}$ (and hence of $P_{\parallel}$) can be found.

(The fact that the net oscillatory field at the nucleus may be oppositely directed to the external oscillatory field (see end of § 4.1) does not cause any complication, here, since both must rotate in the same sense.)

In cases where an ion with $S = \frac{1}{2}$ interacts with two nuclear spins, information concerning the relative signs of the two hyperfine parameters can be obtained by driving two Endor transitions simultaneously (see Cook and Whiffen 1964, 1965).

$S > \frac{1}{2}$, axial symmetry, magnetic dipole and electric quadrupole hyperfine structure

The more general case of $S > \frac{1}{2}$ can now be disposed of quite simply. From eqns (3.54) and (3.62) the Endor quantum for the transition $m \leftrightarrow m-1$ is

$$|h\nu_n| = AM+(A_\parallel A_\perp^2/2AG)\{M^2-S(S+1)\}-G_I+P(2m-1)- \\ -M(2m-1)\left\{(A_\parallel^2+A^2)(A_\perp^2/4A^2G)+\frac{(A_\parallel^2-A_\perp^2)^2}{8A^2G}\left(\frac{g_\parallel g_\perp}{g^2}\right)^2 \sin^2 2\theta\right\}, \quad (4.5)$$

which differs only from our previous expressions in that the second term contains the quantity $\{M^2-S(S+1)\}$, which is just $-\frac{1}{2}$ for $S = \frac{1}{2}$. This means that we can separate this term from G_I by making measurements using different electronic transitions, without needing to make measurements at two different e.s.r. frequencies. The Endor transitions for different values of $|M|$ come at very different frequencies, and there is no difficulty in identifying the value of $|M|$ concerned. As regards signs, the Endor spectrum yields (as before) the sign of $g_\parallel^{(I)}$ relative to that of $g_\parallel$, and the sign of $P_\parallel$ relative to that of $A_\parallel$. However the sign of the fine-structure terms can be found by measurements of the e.s.r. spectrum at low temperatures, and hence the sign of $A_\parallel$ from the second-order effects in the e.s.r. spectrum, as described in §§ 3.3, 3.6. In this case the sign of $P_\parallel$ can be established.

In eqn (4.5) the second-order terms in P^2/A have been omitted; in fact they vanish if measurements are made along the unique axis. It is almost essential to make Endor measurements along such an axis for reasons of precision. Not only are the off-diagonal terms tiresome to evaluate (though this can be done by a computer), but they cannot be evaluated correctly unless the exact orientation of the external magnetic field relative to the crystal axes is known (which cannot be found by a computer). When $S > \frac{1}{2}$, the second-order terms of the type considered in § 3.10, which are of order $(A/G) \times$ (fine structure parameter), become of tremendous importance and must be eliminated by careful alignment of the crystal so that the external magnetic field is exactly along a principal axis. Experimentally, the alignment of the crystal can be checked directly in the e.s.r. spectrum by observing the intensity of the 'forbidden' transitions due to these second-order terms, and adjusting the orientation to make their intensity as small as possible. With exact alignment they should vanish, and in practice the degree of mis-alignment can be estimated from their intensity, so that the resultant error in the Endor measurement can be gauged and, in

favourable cases, reduced to an insignificant amount. For example, Baker and Hurrell (1963) estimate that misalignment by 0·1° could produce an unresolved splitting of 40 kHz in Endor of Eu^{2+} in CaF_2. A ligand Endor spectrum can also be used to obtain exact alignment (see Bessent and Hayes 1965, Davies and Hurrell 1968).

In this connection, measurement of the Endor transitions using the highest possible frequency for observation of the e.s.r. spectrum is clearly very desirable because

(i) second-order terms arising from matrix elements between different electronic levels become less important, since the energy in the denominators of a perturbation expansion is maximized; thus alignment of the crystal becomes less critical. In addition, line widths are reduced, as mentioned in § 4.10;

(ii) in many Endor experiments the prime motive is determination of $g^{(I)}$ through measurement of the energy G_I which is linearly proportional to H. The value of $g^{(I)}$ can therefore be measured with greater accuracy if a high e.s.r. frequency (larger magnetic field) is used. Obviously this does not help to separate the true g_I from the pseudo-nuclear Zeeman terms, and since these are largest when there are nearby electronic levels they can then be calculated accurately only if the electronic states and levels are known rather well.

The importance of the pseudo-nuclear Zeeman terms can be seen from a rough estimate. The change in frequency that they produce in a nuclear transition is of order $\nu_e(A/\Delta)$, where ν_e is the microwave frequency, A the hyperfine constant, and Δ the energy of the relevant excited state. Taking $\nu_e = 10^{10}$ Hz, we need (A/Δ) to be less than 10^{-6} if the shift is not to exceed the line width, which may be only 10^4 Hz. This inequality is fulfilled usually only for a half-filled shell such as d^5 or f^7, where A is unusually small and Δ exceptionally large. In an extreme case such as Ho^{2+} in CaF_2, which has a low-lying excited state at about 30 cm^{-1} (see Lewis and Sabisky (1963)), the apparent value of $g^{(I)}$ is some forty times larger than the true value of g_I.

4.3. Enhancement of the nuclear transition probability

We consider now the question of the nuclear transition probability, since this is important if the nuclear transition rate is to compete with spin-lattice relaxation processes that are electronic rather than nuclear in origin. In addition to the direct coupling of the oscillatory field with the nuclear magnetic moment, we have two other effects:

(a) the pseudo-nuclear Zeeman effect, discussed in § 1.8(e), § 3.7, and more fully in § 18.1; this arises from the admixture of excited

states by the electronic Zeeman interaction, and in some cases can be much larger than the true nuclear Zeeman interaction (cf. §§ 4.2 and 4.8);

(b) modulation of the electronic hyperfine field by the applied oscillatory field, as outlined at the end of § 4.1.

In fact both these effects are essentially similar; we can incorporate (a) with the direct nuclear Zeeman interaction by using the same approach as in the static spin Hamiltonian, and follow this by a separate calculation of (b).

On this basis, the modified nuclear Zeeman effect is written in the form (cf. eqn (3.42))

$$\mathscr{H} = -\beta(\mathbf{H} \cdot \mathbf{g}^{(I)} \cdot \mathbf{I}) = -\beta(g_x^{(I)} H_x I_x + g_y^{(I)} H_y I_y + g_z^{(I)} H_z I_z), \quad (4.6)$$

where (x, y, z) are the principal axes of the nuclear 'g-tensor', which includes the direct interaction with the nuclear moment as well as the 'pseudo-nuclear' Zeeman interaction. For simplicity, we take not the most general case of an arbitrary orientation of the static field $\mathbf{H}$, but (as in § 3.2) assume $\mathbf{H}$ lies in the plane $y = 0$ at an angle θ to the z-axis (cf. Fig. 3.1). We assume that all tensor quantities have the same principal axes, and allow all principal values to be unequal; however, if the principal values for the x, y axes are equal, so that the z-axis is the unique symmetry axis, there is no loss of generality in our assumption about $\mathbf{H}$ since we can always choose the x-axis so that $\mathbf{H}$ lies in the xz-plane. Without appreciable danger of confusion, we call the nuclear oscillatory field $\mathbf{H}_1$, and assume it to be linearly polarized in a direction making an angle η with the y-axis, whose projection on the xz-plane makes an angle θ_1 with the z-axis (cf. § 3.2). Then the components of $\mathbf{H}_1$ are

$$\left.\begin{aligned} H_x &= H_1 \sin\eta \sin\theta_1, \\ H_y &= H_1 \cos\eta, \\ H_z &= H_1 \sin\eta \cos\theta_1. \end{aligned}\right\} \quad (4.7)$$

In a strong steady magnetic field $\mathbf{H}$, we diagonalize the static Hamiltonian as in Fig. 3.10 by rotating the nuclear axes about the y-axis through an angle ψ, a procedure that is appropriate if the magnetic hyperfine term dominates the nuclear Zeeman interaction; then

$$\begin{aligned} I_x &= I'_x \cos\psi + I'_z \sin\psi, \\ I_y &= I'_y, \\ I_z &= -I'_x \sin\psi + I'_z \cos\psi, \end{aligned} \quad (4.8)$$

where the primes refer to the axes (x_n, y_n, z_n) and

$$\cos\psi = \left(\frac{g_z A_z}{gA}\right)\cos\theta, \quad \sin\psi = \left(\frac{g_x A_x}{gA}\right)\sin\theta. \tag{4.9}$$

Our oscillatory nuclear Zeeman interaction then becomes, combining eqns (4.6)–(4.9),

$$-\beta H_1 \begin{bmatrix} I'_x\{(g_x^{(I)} g_z A_z/gA)\cos\theta\sin\theta_1 - (g_z^{(I)} g_x A_x/gA)\sin\theta\cos\theta_1\}\sin\eta + \\ +I'_y g_y^{(I)}\cos\eta + \\ +I'_z\{(g_x^{(I)} g_x A_x/gA)\sin\theta\sin\theta_1 + (g_z^{(I)} g_z A_z/gA)\cos\theta\cos\theta_1\}\sin\eta \end{bmatrix}. \tag{4.10}$$

The rate at which nuclear transitions are induced is proportional to the sum of the squares of the coefficients of I'_x, I'_y so that by analogy with eqns (3.8a) and (3.16) we can define an oscillatory nuclear g-factor $g_1^{(I)}$ whose value is given by

$$(g_1^{(I)})^2 = \sin^2\eta\left\{\left(\frac{g_x^{(I)} g_z A_z}{gA}\right)\cos\theta\sin\theta_1 - \left(\frac{g_z^{(I)} g_x A_x}{gA}\right)\sin\theta\cos\theta_1\right\}^2 + \\ +\cos^2\eta(g_y^{(I)})^2. \tag{4.11}$$

It is clearly best to make either $\sin\eta$ or $\cos\eta = 1$, according to which of the multiplying factors is the larger. In the former case the optimum value of θ_1 is given by

$$\tan\theta_1 = -\left(\frac{g_x^{(I)} g_z A_z}{g_z^{(I)} g_x A_x}\right)\cot\theta = -\left(\frac{g_x^{(I)}}{g_z^{(I)}}\right)\cot\psi, \tag{4.12}$$

so that the optimum value of θ_1 is $\psi+\pi/2$ if there is no anisotropy in $g^{(I)}$, as we should expect, and $\theta+\pi/2$ if there is no anisotropy in $g^{(I)}$, g, or A.

We now consider the effect of $\mathbf{H}_1$ acting through the electronic magnetization and the hyperfine interaction. From eqns (3.8a) and (3.15) the electronic oscillatory spin Hamiltonian is

$$\mathscr{H}_1 = \beta H_1(g_{1x}S'_x + g_{1y}S'_y + g_{1z}S'_z), \tag{4.13}$$

where

$$\begin{aligned} g_{1x} &= (g_x g_z/g)\sin\eta, \quad g_{1y} = g_y\cos\eta, \\ g_{1z} &= \{(g_x^2 - g_z^2)/2g\}\sin 2\theta\sin\eta \end{aligned} \tag{4.14}$$

if we assume that $\theta_1 = \theta+\pi/2$, so that $\mathbf{H}_1$ is normal to $\mathbf{H}$. The primes on the components of $\mathbf{S}$ indicate that these refer to the axes (x_e, y_e, z_e) in which the static electronic Zeeman interaction is diagonal (see § 3.2).

Since we are interested only in nuclear transitions that depend on the components I'_x, I'_y, we combine (4.13) with the relevant part of the hyperfine interaction, which from (3.52) is

$$(A_xA_z/A)S'_xI'_x+A_yS'_yI'_y. \tag{4.15}$$

In the combination we use the terms S'_+, S'_- from (4.13) and (4.15), and vice versa to obtain terms diagonal in S'_z, which are found to be altogether

$$\tfrac{1}{2}\beta H_1\{I'_xg_{1x}(A_xA_z/A)+I'_yg_{1y}A_y\}\left\{\frac{S(S+1)-M(M+1)}{W_M-W_{M+1}}+\right.$$
$$\left.+\frac{S(S+1)-M(M-1)}{W_M-W_{M-1}}\right\}, \tag{4.16}$$

and if we assume that $W_M-W_{M-1} = -(W_M-W_{M+1}) = g\beta H$, (4.16) reduces to

$$\mathscr{H}_1 = \frac{MH_1}{H}\left\{I'_x\left(\frac{g_xg_z}{g^2}\right)\left(\frac{A_xA_z}{A}\right)\sin\eta+I'_y\left(\frac{g_y}{g}\right)A_y\cos\eta\right\} \tag{4.17}$$

on substituting for g_{1x}, g_{1y} and omitting the term in I'_z.

To be strictly logical we should add the coefficients of I'_x, I'_y in (4.17) to those in (4.10) (with $\theta_1 = \theta+\pi/2$), and take the sum of the squares of the resultant coefficients to give a net value of $(g_1^{(I)})^2$. However the two mechanisms are so disparate in size that this is hardly worth while. Clearly we should again make $\sin\eta$ or $\cos\eta = 1$ in (4.17), according to which coefficient is the larger, and with high anisotropy they can be quite different in magnitude. In the absence of anisotropy (4.17) and (4.10) with $\theta_1 = \theta+\pi/2$ add to

$$\mathscr{H}_1 = H_1\{-g^{(I)}\beta+(AM/H)\}(I_x\sin\eta+I_y\cos\eta), \tag{4.18}$$

where the coefficient $H_1(AM/H)$ is just equivalent to the classical value deduced at the end of § 4.1, which would correspond to an oscillatory Hamiltonian

$$\mathscr{H}_1 = -g_I\beta H_1(H_e/H)(I_x\sin\eta+I_y\cos\eta), \tag{4.18a}$$

since $g_I\beta H_e = -AM$, by comparison with eqn (1.28).

If we refer to the formulae used to derive the static pseudo-nuclear Zeeman effect (e.g. eqn (1.97)), we can see that the mechanisms involved in deducing eqns (4.10) and (4.16) are basically similar. The oscillatory electronic Zeeman interaction induces an oscillatory component in the electronic magnetic moment (by admixture of other electronic states) proportional to H, which then interacts with the nuclear magnetic

moment through the magnetic hyperfine interaction. In general, (4.16) gives the larger effect, because the admixed electronic state comes from a level only distant $g\beta H$ in energy, whereas (4.10) involves levels separated by a ligand field splitting (or other larger interactions). If the ligand field leaves low-lying excited states, and we apply a static field H such that $g\beta H$ becomes comparable with the energy of another ligand field state, the two expressions (4.10), (4.16) will become comparable in magnitude, since the energy denominators required in the perturbation theory will be of the same order. We have also inherently assumed that $H_e \gg H$, since essentially we diagonalized the hyperfine interaction (as far as possible) by choosing nuclear axes such that z_n is parallel to H_e. If H_e and H are comparable in magnitude (as often occurs in ligand hyperfine structure), we should use a more sophisticated approach analogous to that in § 3.11 following eqn (3.81). However the enhancement factor for the nuclear transition probability is then relatively small, and usually of insufficient importance to justify a more elaborate calculation. We content ourselves by remarking that the optimum direction of H_1 for an Endor nuclear transition, if $g^{(I)}$ is isotropic, is simply normal to the appropriate vector K_M in Fig. 3.19.

From eqn (2.51), the rate at which nuclear transitions are induced between levels m and $m \pm 1$ is

$$w_n = \frac{\pi}{2}\left(\frac{g_1^{(I)}\beta H_{1n}}{\hbar}\right)^2 \{I(I+1) - m(m\pm 1)\} f(\omega), \tag{4.19}$$

where we have written (H_{1n}) to remind ourselves that this must be at the nuclear (Endor) frequency, and $(g_1^{(I)})^2$ is given by (4.11) modified to include the analogous terms from (4.17). $f(\omega)$ is the appropriate shape function, which we take to be that of a spin packet; if the half width at half intensity of the latter is $(\Delta\omega/2\pi)$, then at the centre of the Endor line we have from (2.65) for a narrow line, $f(\omega) = 1/(\pi\Delta\omega) = \tau_2/\pi$.

Use of a circularly polarized nuclear field

When we have anisotropy and the steady field **H** is in an arbitrary direction, analysis of the Endor signal resulting from the use of a circularly polarized nuclear oscillatory field is exceedingly tedious, and not worth while in view of the fact (see § 4.2) that accurate measurements are made usually with **H** along a principal axis. We therefore assume that **H** is along the z-axis, and that $\mathbf{H}_{1n}$ is normal to it; however we do not assume that we have axial symmetry about the z-axis, since the analysis is then applicable to the x, y axes by using a cyclical

interchange $x \rightarrow y \rightarrow z$. The oscillatory nuclear Hamiltonian is then, instead of eqn (4.6),

$$\begin{aligned}\mathscr{H}_{1n} &= -\beta H_{1n}(g_x^{(I)} I_x \cos \omega t + g_y^{(I)} I_y \sin \omega t) \\ &= -\tfrac{1}{4}\beta H_{1n}\begin{bmatrix} I_+\{(g_x^{(I)} - g_y^{(I)})e^{i\omega t} + (g_x^{(I)} + g_y^{(I)})e^{-i\omega t}\} + \\ + I_-\{(g_x^{(I)} + g_y^{(I)})e^{i\omega t} + (g_x^{(I)} - g_y^{(I)})e^{-i\omega t}\}\end{bmatrix}, \quad (4.20a)\end{aligned}$$

where we have used a transformation similar to that between eqns (3.17) and (3.18).

The operator I_- induces the transition $m \rightarrow m-1$, for which the required energy is (in first order)

$$W_m - W_{m-1} = A_z M - g_z^{(I)} \beta H + \tfrac{3}{2} P_z (2m-1),$$

which may be positive or negative. By an analysis similar to that following eqn (3.18) we find that the rates at which nuclear transitions are induced vary as follows.

Sign of	Transition rates are proportional to	
$A_z M - g_z^{(I)} \beta H + \tfrac{3}{2} P_z (2m-1)$	Right-hand sense	Left-hand sense
positive	$(g_x^{(I)} + g_y^{(I)})^2$	$(g_x^{(I)} - g_y^{(I)})^2$
negative	$(g_x^{(I)} - g_y^{(I)})^2$	$(g_x^{(I)} + g_y^{(I)})^2$

This table shows that the sign of $W_m - W_{m-1}$ (and hence of the largest term in this energy) can be found by observing the Endor intensities with right- and left-handed nuclear signals, provided the relative signs of $g_x^{(I)}$ and $g_y^{(I)}$ are known.

If the oscillatory field inducing nuclear transitions is due primarily to the effect of 'stirring' the hyperfine field rather than to direct interaction with the nuclear moment, the oscillatory Hamiltonian under the conditions assumed above is

$$\mathscr{H}_{1n} = (M/H) H_1 \{I_x A_x (g_x/g_z) \cos \omega t + I_y A_y (g_y/g_z) \sin \omega t\}, \quad (4.20b)$$

from which a similar table is readily constructed, and it is apparent that we need to know the relative signs of $(g_x A_x)$ and $(g_y A_y)$.

If we have axial symmetry about the z-axis, then

$$(g_x^{(I)} - g_y^{(I)}) = (g_x A_x - g_y A_y) = 0$$

and only one sense of the nuclear circularly polarized signal is effective. If $A_z M$ is the largest term in $W_m - W_{m-1}$, this gives the sign of $A_z = A_\parallel$ (those of $A_x = A_y = A_\perp$ are indeterminate).

4.4. Endor on donors in silicon

The method of Endor was invented by Feher (1956*b*), and it is fitting that we should start discussion of experimental work by outlining his comprehensive and elegant experiments on donors in silicon. As we do not discuss elsewhere shallow traps in semiconductors, we give here a very brief resumé of the essential features. The donors used are principally the group V atoms P, As, Sb, which have one electron more in their outer shells than silicon. When these atoms replace a silicon atom in the silicon lattice, four of the outer electrons are used in forming bonds with the four immediate silicon neighbours of the diamond-type lattice, as in the case of a silicon atom itself. The extra electron of the group V atom may remain attached to the donor, giving it one unpaired electron spin; or it may be excited in to the conduction band to act as a conduction electron, in which case the ionized impurity atom is left with one net positive charge and no unpaired electron spins. The 'ionization potentials' required for this process are given in Table 4.1;

TABLE 4.1

Data of Feher (1959) for three group V donors in silicon. V_i is the ionization potential to the conduction band; g the spin resonance g-factor relative to that $g_c = 1{\cdot}99875(10)$ for conduction electrons in a more highly doped sample, A is the magnetic hyperfine constant for the isotope whose mass and nuclear spin are also given

Donor atom	V_i meV	$g-g_c$	Isotope mass	$\|A\|$ (MHz)	Nuclear spin
Sb	39	$-1{\cdot}7(1)\times10^{-4}$	121	186·802(5)	$\frac{5}{2}$
			123	101·516(4)	$\frac{7}{2}$
P	44	$-2{\cdot}5(1)\times10^{-4}$	31	117·53(2)	$\frac{1}{2}$
As	49	$-3{\cdot}8(1)\times10^{-4}$	76	198·35(2)	2

since for room temperature the equivalent voltage ($eV = kT$) is about 25 mV, the electrons will be practically all in the lower energy state, bound to their parent donor atoms, at helium temperatures. The substance is then a good electrical insulator so long as the donor concentrations are of order 10^{16} cm^{-3}, as used in Feher's experiments; conduction electrons occur in more highly doped samples, with donor concentrations $\sim10^{18}$ cm^{-3}, and give a narrow homogeneously broadened electron spin resonance line.

The ground state of the extra electron attached to a donor is $^2S_{\frac{1}{2}}$, though its wave-function is very much more extended than in a free

atom and has a finite density at many neighbouring silicon nuclei. The electron spin resonance spectrum occurs at a g-value very close to the free electron value, and shows hyperfine structure due to interaction both with the nuclear magnetic moment of its parent donor and with the nuclear moments of silicons on neighbouring lattice sites provided these are occupied by the odd isotope ^{29}Si, for which $I = \frac{1}{2}$, and whose natural abundance is about 5 per cent. The effective spin Hamiltonian for the electron bound to its parent donor is therefore ($S = \frac{1}{2}$)

$$\mathscr{H} = g\beta(\mathbf{H} \cdot \mathbf{S}) + A(\mathbf{S} \cdot \mathbf{I}) - g_I\beta(\mathbf{H} \cdot \mathbf{I}), \tag{4.21}$$

where g, A are isotropic and g_I is the true nuclear g-factor. To this we must add the interaction with neighbouring ^{29}Si nuclei for which, with $I = \frac{1}{2}$, we have

$$\mathscr{H}_L = \sum_L \{A^L(\mathbf{S} \cdot \mathbf{I}^L) - (g_I)^L\beta(\mathbf{H} \cdot \mathbf{I}^L)\} + \sum_L A_p^L(3S_{z'}I_{z'}^L - \mathbf{S} \cdot \mathbf{I}^L), \tag{4.22}$$

where the summation is over all lattice sites L occupied by ^{29}Si nuclei. The first term in (4.22) represents the interaction arising from the electron density of s-like character at the ^{29}Si nucleus due to the donor electron; the second is the ^{29}Si nuclear Zeeman interaction in the external field $\mathbf{H}$; and the third arises from magnetic dipole interaction between the ^{29}Si nuclear moment and the extended electron spin magnetization of the donor electron, the direction z' being that line joining the donor nucleus to the ^{29}Si nucleus at lattice site L. In a strong external magnetic field $\mathbf{H}$ the energy levels are approximately

$$\begin{aligned} W = {} & g\beta HM + AMm - g_I\beta Hm + \\ & + \sum_L [\{A^L M - (g_I)^L\beta H\}m^L + A_p^L M^L(3\cos^2\theta - 1)m^L], \end{aligned} \tag{4.23}$$

where θ is the angle between H and the z'-axis, and the approximation we have made is that $A_p^L \ll A^L$.

In an ordinary electron resonance transition

$$(M, m, m^L) \leftrightarrow (M-1, m, m^L)$$

we have for $M = \frac{1}{2}$,

$$h\nu_e = g\beta H + Am + \sum_L \{A^L + A_p^L(3\cos^2\theta - 1)\}m^L, \tag{4.24}$$

in which the hyperfine splitting Am due to the donor nucleus is usually well resolved, while that from the remaining terms due to the ^{29}Si nuclei is not and gives an inhomogeneously broadened line. The nuclear

(Endor) transitions occur for $\Delta M = \Delta m^L = 0$, $\Delta m = \pm 1$, giving

$$h\nu_n^{\pm} = |A/2 \mp g_I \beta H| \tag{4.25}$$

for the donor nucleus, and for the silicon nuclei at $\Delta M = \Delta m = 0$, $\Delta m^L = \pm 1$, giving

$$h\nu_L^{\pm} = |-(g_I)^L \beta H \pm A^L/2 \pm \tfrac{1}{2} A_p^L (3\cos^2\theta - 1)|, \tag{4.26}$$

where the $\pm$ signs refer to the electronic states $M = \pm\frac{1}{2}$ respectively. The frequencies (4.25) are close to the values of A given in Table 4.1, while the frequencies (4.26) give two sets of lines around

$$(g_I)^L \beta H/h = 2{\cdot}6 \text{ MHz}$$

at $H = 3000$ G, and the A^L, A_p^L terms range from a few MHz for nearby ^{29}Si nuclei down to zero for the more distant nuclei.

Because of the very long spin-lattice relaxation times in silicon ($\tau_1 \sim 1$ h), it is possible to carry out either adiabatic rapid passage experiments or saturation experiments, both for the electronic and nuclear transitions (cf. §§ 1.12, 1.13). In the work of Feher (1959), a small part of the inhomogeneously broadened line was saturated by a high-power pulse, so that a 'hole was burnt' in the line, as shown in Fig. 4.4, since only the spin packets within that part of one hyperfine line at the resonance frequency were saturated. If the electron resonance signal at this same frequency is now monitored at a low level, the

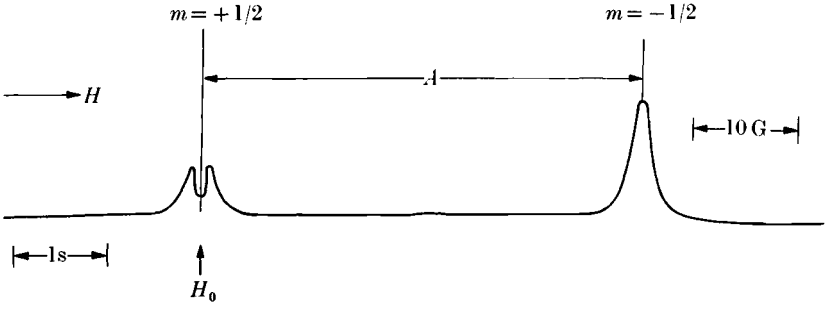

FIG. 4.4. 'Burning a hole' in the electronic transition $(+\frac{1}{2}, +\frac{1}{2}) \leftrightarrow (-\frac{1}{2}, +\frac{1}{2})$ for phosphorus donors in silicon. After a strong saturating pulse is applied at H_0, the electronic magnetic resonance signal is traversed at low power level, to show that only the spin packets at the resonance frequency for the saturating signal are affected. If the electron resonance signal at this frequency is monitored at low level, an increase in signal is observed when Endor transitions at either the donor or ^{29}Si frequencies are induced. A is the hyperfine splitting for the ^{31}P donor ($I = \frac{1}{2}$) nuclei; the inhomogeneous line width is due to interaction with the nuclear moments of ^{29}Si nuclei ($I = \frac{1}{2}$) on neighbouring lattice sites. The time scale for the traverse at low power level is indicated at bottom left, and the magnetic field scale at the right. (After Feher 1959.)

application of a strong oscillatory field at either ν_n or ν_L will cause a change in level. This will be of order $\delta_e/2$ if the populations of the two nuclear levels involved are inverted by an adiabatic rapid passage experiment, or of order $\delta_e/4$ if the populations are equalized through saturation. The two alternatives are illustrated in Fig. 4.5.

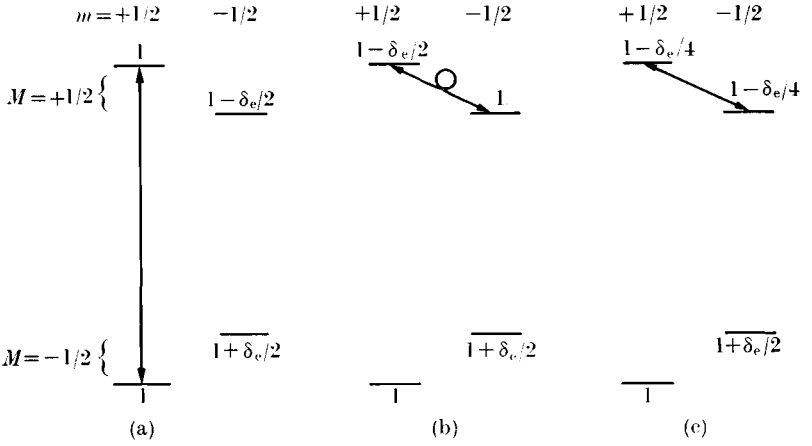

FIG. 4.5. Level populations in an Endor experiment before spin-lattice relaxation can act to restore thermal equilibrium.
(a) After the electronic transition $(+\frac{1}{2}, +\frac{1}{2}) \leftrightarrow (-\frac{1}{2}, +\frac{1}{2})$ has been saturated. (b) Inversion of the nuclear populations in the $M = +\frac{1}{2}$ states following adiabatic rapid passage through the Endor $(+\frac{1}{2}, +\frac{1}{2}) \leftrightarrow (+\frac{1}{2}, -\frac{1}{2})$ transition. (c) Equalization of the populations in the $M = +\frac{1}{2}$ states following saturation of the same Endor transition. The levels are drawn for the system $S = I = \frac{1}{2}$. Similar effects are obtained by saturating the other electronic transition followed by adiabatic rapid passage through or saturation of the other Endor transition.

In the process of burning a hole in the line we are saturating just those spin packets consisting of electron spins that experience a given local field from the neighbouring silicon nuclei. When Endor transitions are induced which change the orientation of these neighbouring nuclei, the local field will be altered both for the saturated packets and also for unsaturated spin packets consisting of other electron spins to which the same nuclei are also neighbours. Effectively this transfers neighbouring spin packets into and out of the hole, thus giving an increased electron resonance signal again. This is known as a 'packet-shifting' mechanism; from eqn (4.23) we see that an Endor transition $\Delta m^L = \pm 1$ just changes the local field at a donor relative to which the ^{29}Si nucleus occupies lattice site L by an amount

$$|M\{A^L + A_p^L(3\cos^2\theta - 1)\}/g\beta|, \tag{4.27}$$

which is just the difference between the Endor frequency (4.26) ν_L and the ordinary nuclear resonance frequency $(g_I)^L\beta H/h$, divided by $(g\beta/h)$.

A typical Endor experiment of Feher (1959) is shown in Fig. 4.6, the electron resonance being observed at 9000 MHz and $T = 1{\cdot}25°\text{K}$.

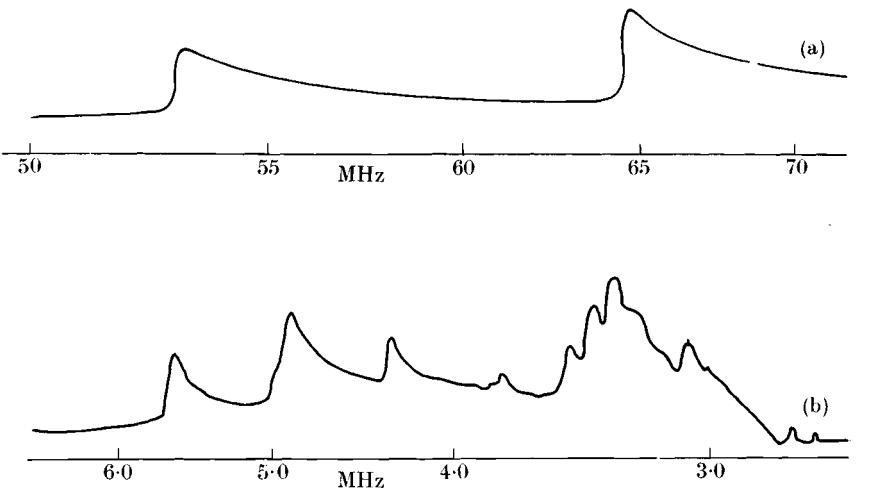

FIG. 4.6. Change in the electron resonance signal at 9000 MHz and $T = 1{\cdot}25°\text{K}$ due to phosphorus (^{31}P) donors in silicon, upon application of power at the Endor frequencies. (a) Traverse through the ^{31}P Endor spectrum; the two frequencies correspond to those in eqn (4.25). (b) Traverse through the high frequency side of the ^{29}Si spectrum; the frequencies correspond to those in (4.26) with the lower (−) sign before A^L. Another line is observed around 2·7 MHz, due to more distant ^{29}Si for which A^L is small (after Feher 1959).

The upper diagram (Fig. 4.6a) shows the increase in electron spin resonance signal obtained by traversing the Endor transitions for the donor nucleus ^{31}P, which also has $I = \frac{1}{2}$. These transitions are given by eqn (4.25). Because the Endor line width is only 10 kHz, there is a sharp rise at the front, due to the sudden increase in population difference between the two previously saturated electron levels, followed by a slow recovery towards a steady-state condition. The second Endor transition is more intense for the following reason. From Fig. 4.5(b) it can be seen that adiabatic rapid passage through one Endor transition gives a population difference $\delta_e/2$ between the two electron levels for $m = +\frac{1}{2}$; if this is followed quickly by adiabatic rapid passage through the other Endor transition, the populations of the two $M = -\frac{1}{2}$ levels will be inverted, giving a net population difference between the $m = +\frac{1}{2}$ levels of δ_e. Thus the second Endor transition should be twice as intense as

the first if they are traversed in a time too short for the populations to recover towards steady state values.

The hyperfine parameters for the donor nuclei are given in Table 4.1, and illustrate the accuracy that can be obtained in Endor experiments. The ratio of the two values of A for the isotopes 121, 123 of antimony is not quite equal to the ratio of the nuclear moments, and yields a hyperfine anomaly (cf. eqn 17.91, § 17.7) of $\Delta = -(0{\cdot}352 \pm 0{\cdot}005)$ per cent, where

$$\frac{A(121)}{A(123)} = \frac{g_I(121)}{g_I(123)}(1+\Delta). \tag{4.28}$$

The ratio of the hyperfine constants was found to be 1·84012(1) in the Endor experiments (Eisinger and Feher (1958)), while separate nuclear magnetic resonance measurements gave 1·84661(1) for the ratio of the g_I values.

The g-values for the various donors were measured by comparison with that g_c arising from magnetic resonance of conduction electrons in a more heavily doped sample (3×10^{18} P/cm^3), for which the value of $g_c = 1{\cdot}99875(10)$ was determined separately by comparison with a proton magnetic resonance signal. The value of $|(g-g_c)|$ increases with the value of V_i (see Table 4.1), where V_i is the 'ionization potential' required to lift the donor electron into the conduction band.

The Endor transitions due to ^{29}Si lattice sites are shown in Fig. 4.6(b). Here it is possible to identify the lattice sites involved through the anisotropy due to the A_p^L term in (4.26) by plotting the line frequency as a function of the orientation of the external field **H**, and using the relative intensity variation arising from the number of equivalent lattice sites giving an Endor transition at the same frequency. These experiments form an important method of checking the theory of shallow donors in semiconductors and measuring the parameters involved, details of which may be found in Feher (1959).

From the values of A^L, A_p^L determined for the various lattice points by means of Endor, it is possible to calculate both the shape and the width of the inhomogeneously broadened electron resonance line, and good agreement was obtained (Feher (1959)).

4.5. Endor on donors in silicon—relaxation effects

We now consider briefly relaxation effects in Endor, starting in this section with the experimental work of Feher and Gere (1959) on donors in silicon, in particular ^{31}P, which has $I = \frac{1}{2}$. Since the donor electron has $S = \frac{1}{2}$, we are dealing with the smallest possible number of energy

levels, two electronic and two nuclear. The various relaxation processes that are operative in such a system are indicated in Fig. 4.9(a). The simple electron spin relaxation processes ($\Delta M = \pm 1$, $\Delta m = 0$) follow the broken vertical lines, with characteristic times τ_1 which are the same for either hyperfine line. One broken sloping line represents a process involving both an electronic 'flip' and a nuclear 'flop' such that $\Delta(M+m) = 0$, with a characteristic time τ_x. The other two broken sloping lines represent relaxation effects within the nuclear spin system for which $\Delta M = 0$, $\Delta m = \pm 1$, with characteristic time τ_n which is essentially the same for either nuclear transition. The remaining path for which $\Delta(M+m) = 2$ is not allowed when the hyperfine interaction is isotropic—see eqn (4.32).

In the experiments of Feher and Gere the level populations were disturbed from the values appropriate to thermal equilibrium, either by saturating one transition or more, or by adiabatic rapid passage through one line or more to reverse the populations. The latter proved more convenient when dealing with relaxation times longer than about a second. Special methods were devised of disturbing the equilibrium populations in different ways so as to disentangle the various relaxation processes (see below). The relaxation time was then determined by observing the exponential recovery of the populations towards the thermal equilibrium values, by monitoring the electron resonance signal at low level.

The first experiments were simple electron magnetic resonance experiments to determine τ_1, usually the fastest of all the relaxation times. It was found that the value of τ_1 was concentration dependent above about 10^{16} P/cm^3, and concentration independent below this level. In the latter case τ_1 was proportional to $(1/T)$, typical of a direct relaxation process (see § 1.11 and Chapter 10), below 2°K, the value of τ_1 lying in the range 10^{+3} to 10^{+4} s (about 1 h). A much faster rate of change of τ_1 with temperature set in above 2°K.

When the value of τ_x is very much longer than that of τ_1, it is necessary to adopt a method of measuring it that avoids the short-circuiting effect of the τ_1 paths. This method is to saturate both electronic transitions, so that all population differences of order δ_e are removed as shown in Fig. 4.7(a). If this situation is retained for a time of order τ_x, relaxation via the sloping relaxation path tends to re-establish the normal population difference between the $(+\frac{1}{2}, -\frac{1}{2})$ and $(-\frac{1}{2}, +\frac{1}{2})$ levels, the saturating signal causing the populations of the other two levels to follow, as in Fig. 4.7(b). If the saturating power is

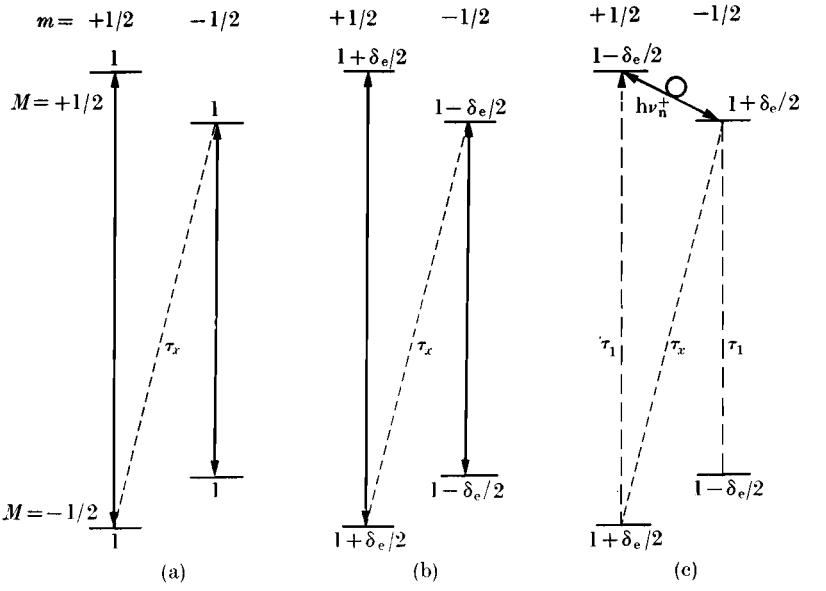

FIG. 4.7. Illustrating the method of Feher and Gere (1959) for measuring τ_x. (a) Both electronic transitions are saturated thus initially equalizing all the populations. (b) Saturation of both electronic transitions is maintained, but after a time $\gg \tau_x$ the sloping relaxation path establishes the normal population difference between the $(+\frac{1}{2}, -\frac{1}{2})$ and $(-\frac{1}{2}, +\frac{1}{2})$ levels. (c) Adiabatic rapid passage through the $h\nu_n^+$ transition inverts the populations of the $M = +\frac{1}{2}, m = \pm\frac{1}{2}$ levels. The electronic transitions (at low level) now have the normal intensity, except that the $m = -\frac{1}{2}$ line is reversed in sign. If (c) is carried out at various times after (a), the degree to which τ_x has re-established the population difference between the $(+\frac{1}{2}, -\frac{1}{2})$ and $(-\frac{1}{2}, +\frac{1}{2})$ levels can be found, thus giving the value of τ_x.

now removed, and the nuclear transition $h\nu_n^+$ induced by adiabatic rapid passage, the populations of the two $M = +\frac{1}{2}$ nuclear levels are inverted, as shown in Fig. 4.7(c). A quick sweep through the electronic resonance spectrum then shows one normal line ($m = +\frac{1}{2}$) and one inverted line ($m = -\frac{1}{2}$). By observing the strength of these last signals after waiting various intervals to allow the τ_x relaxation process to take effect, values of τ_x of order 30 h at $H = 3200$ G and 5 h at $H = 8000$ G were estimated, both at $T = 1{\cdot}25$°K.

To estimate τ_n a different trick was employed, involving preferential population of the two nuclear $m = -\frac{1}{2}$ levels. If the system is allowed to reach thermal equilibrium in a high field (8000 G, for which $\delta_e' = h\nu_e'/kT$), and then adiabatic rapid passages are performed, first of the electronic line $m = +\frac{1}{2}$ and then on the nuclear line $M = +\frac{1}{2}$, the populations become as shown in Fig. 4.8(a) and 4.8(b). If the field

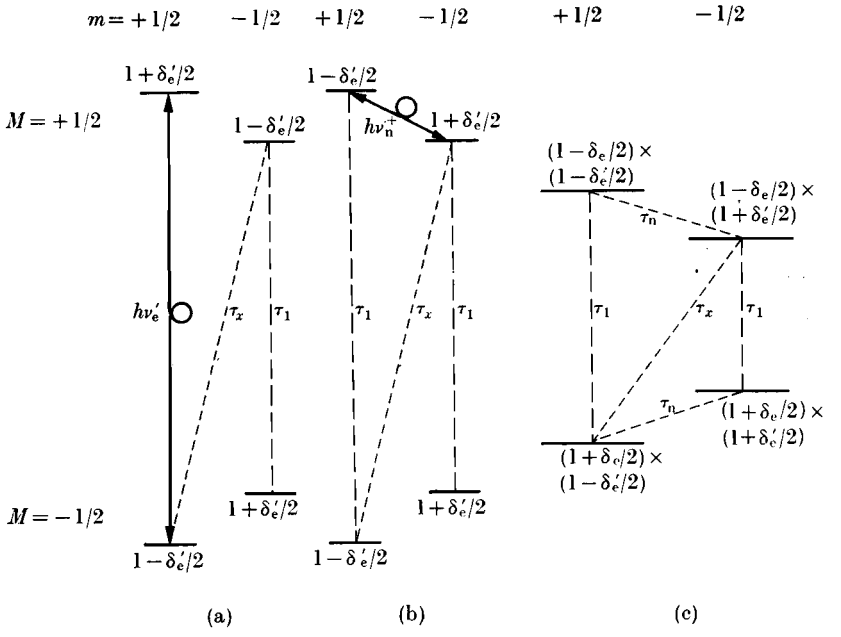

FIG. 4.8. Illustrating the method of Feher and Gere (1959) for measuring τ_n. (a) After thermal equilibrium is reached in a high field ($H = 8000$ G), adiabatic rapid passage of the electronic transition $m = +\frac{1}{2}$ inverts the population of the two $M = \pm\frac{1}{2}$, $m = +\frac{1}{2}$ levels. (b) Adiabatic rapid passage through the $h\nu_n^+$ transition then inverts the population of the $M = +\frac{1}{2}$, $m = \pm\frac{1}{2}$ levels. (c) In a lower field ($H = 3200$ G), relaxation through the rapid τ_1 paths modifies the populations of upper and lower electronic levels by factors $(1-\delta_e/2)$, $(1+\delta_e/2)$ respectively. This can be observed through the unequal strengths of the two electronic transitions which are in the ratio $(1-\delta'_e/2)/(1+\delta'_e/2)$. The relative strengths of these two transitions then return gradually to equality through the relaxation mechanisms τ_x, τ_n. The quantities $\delta'_e = (h\nu'_e/kT)$, $\delta_e = (h\nu_e/kT)$ where ν'_e, ν_e are the electron resonance frequencies in the higher and lower fields respectively.

is now dropped to $H = 3200$ G, for which $\delta_e = h\nu_e/kT$, relaxation through the more rapid τ_1 paths gives the populations shown in Fig. 4.8(c), and the intensity of the two electronic hyperfine lines is in the ratio $(1-\delta'_e/2)/(1+\delta'_e/2)$. This difference is then progressively eliminated as populations return to thermal equilibrium through the τ_x, τ_n processes. As τ_x had been measured separately, a lower limit of $\tau_n \approx 10$ h was established.

When free carriers are present, all these relaxation times are shorter through collisions with the conduction electrons, a process in which a mutual spin flip may occur between donor electron and conduction electron.

4.6. Relaxation effects in Endor—general

Endor experiments on donors in silicon have the unusual feature that the spin-lattice relaxation times are extremely long; in most paramagnetic systems relaxation times of a fraction of a second are the rule. Effects due to adiabatic rapid passage (even if this is feasible) will then vanish in a fraction of a second, and Endor experiments are carried out under steady-state conditions. Signals are somewhat smaller than immediately after a fast transient, but the analysis is rather complex and depends on competition between the various relaxation processes that are operative. An order of magnitude estimate can be obtained as follows for the size of the Endor signal. The relaxation paths for a system with $S = I = \frac{1}{2}$ and an isotropic hyperfine interaction are shown in Fig. 4.9(a). If saturating power is applied to the electronic $m = +\frac{1}{2}$ transition, as in Fig. 4.9(b), the net effect is to 'pump' spins from the lower to the upper of the two $m = +\frac{1}{2}$ levels; the spins can then return to the lower state by phonon emission, either following the direct vertical path τ_1, or by the indirect path via the $(+\frac{1}{2}, -\frac{1}{2})$ state which

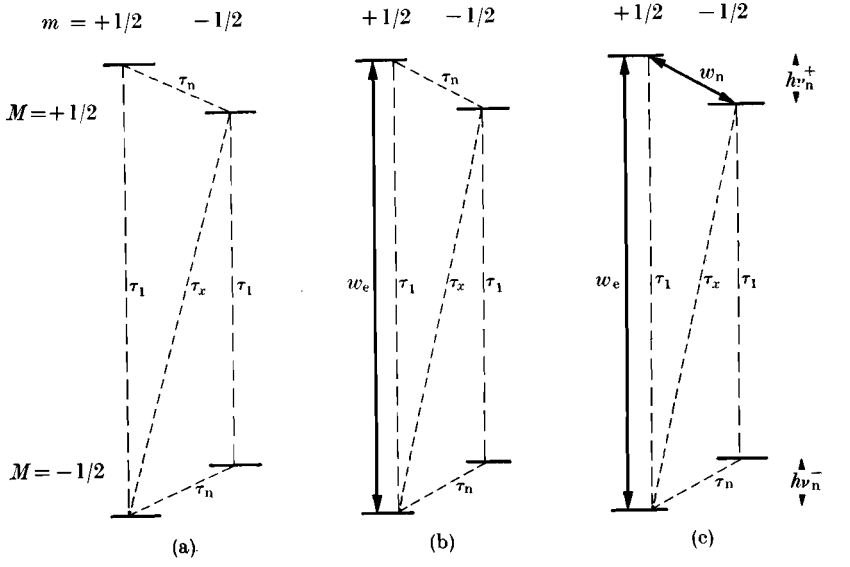

FIG. 4.9. Steady-state Endor signals. (a) Relaxation paths in a system $S = I = \frac{1}{2}$, with an isotropic hyperfine interaction. (b) As in (a), but with an electron resonance signal inducing transitions at a rate w_e on the $\Delta M = \pm 1$, $m = +\frac{1}{2}$ line. (c) As in (b), but with an Endor resonance signal also inducing transitions at a rate w_n on the $M = +\frac{1}{2}$, $\Delta m = \pm 1$ line. In general, $\tau_1 \ll \tau_x \ll \tau_n$, and to be effective in giving an Endor signal we need $w_n \tau_x \geqslant 1$, and not just $w_n \tau_n \geqslant 1$. The reason for this is that the relaxation path τ_n is essentially 'short-circuited' by the much faster indirect paths through τ_x and τ_1 (or w_e), for which the controlling rate is $1/\tau_x$.

involves both τ_n and τ_x and is therefore a very much slower process, controlled by τ_n if this is the longer relaxation time of the two. If power is now also applied to the transition $h\nu_n^+$, transitions to the $(+\frac{1}{2}, -\frac{1}{2})$ level are induced at a rate w_n, and if this is much faster than $1/\tau_x$, the factor controlling return to the $(-\frac{1}{2}, +\frac{1}{2})$ ground state will become τ_x. The net relaxation rate is thus changed from approximately $(1/\tau_1)+(1/\tau_n)$ to $(1/\tau_1)+(1/\tau_x)$, which is a change of order (τ_1/τ_x) in the effective value of τ_1 if $\tau_n \gg \tau_x$, i.e. $(\delta\tau_1/\tau_1) = -(\tau_1/\tau_x)$.

We now use this relation to make an estimate of the change in the electron resonance signal by using the macroscopic equations of Chapter 2 (with our usual reservations as to their validity when dealing with inhomogeneously broadened lines). From eqn (2.75) the electron resonance signal is proportional to $\chi''\sqrt{(P_1)}$, or $\chi''H_1$, where P_1 is the applied power producing an oscillatory field strength H_1. From eqn (2.49) we have

$$\frac{\chi''H_1}{M_0} = -\frac{\gamma H_1 \tau_2}{1+\gamma^2 H_1^2 \tau_1 \tau_2},$$

where for an inhomogeneously broadened line τ_2 is the true spin-spin relaxation time appropriate to the width of a spin-packet. The change in signal resulting from a change $\delta\tau_1$ in τ_1 is

$$\delta\left(\frac{\chi''H_1}{M_0}\right) = \gamma H_1 \tau_2 \left\{\frac{\gamma^2 H_1^2 \tau_1 \tau_2}{(1+\gamma^2 H_1^2 \tau_1 \tau_2)^2}\right\}\frac{\delta\tau_1}{\tau_1}, \tag{4.29}$$

which has its maximum value when $\gamma^2 H_1^2 \tau_1 \tau_2 = 3$. Under this condition we find readily that

$$\frac{\delta(\chi''H_1)}{(\chi''H_1)} = -\frac{3}{4}\frac{\delta\tau_1}{\tau_1} = \frac{3}{4}\frac{\tau_1}{\tau_x}. \tag{4.30}$$

The optimum condition $\gamma^2 H_1^2 \tau_1 \tau_2 = 3$ is somewhat higher than that which gives the maximum electron resonance signal (see eqn (2.49)), and H_1 should be adjusted to this optimum value.

So far we have considered cases where the only important cross-relaxation path is τ_x. This leads to a restriction on the number of Endor signals that we can expect to observe, the reason for which can be understood in two ways. (a) We consider the population differences of order δ_e, and neglect relaxation paths whose times are of order τ_n. Then under complete saturation of the electronic hyperfine transition for $m = +\frac{1}{2}$ we get the populations shown in Fig. 4.10(a), while if the $m = -\frac{1}{2}$ electronic transition is saturated, we get the populations shown in Fig. 4.10(b). A population difference of order δ_e exists in Fig.

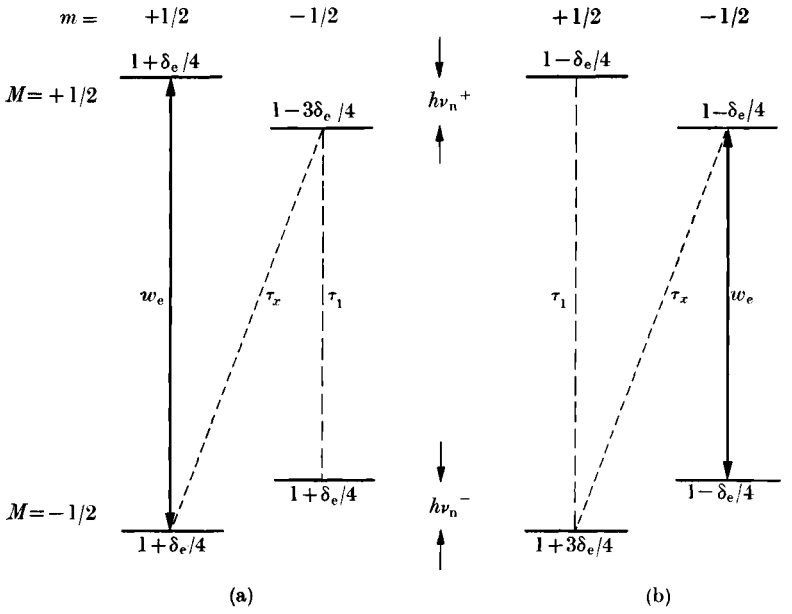

FIG. 4.10. Populations of the levels for the system $S = I = \frac{1}{2}$ in the steady state resulting from saturation of (a) the electronic hyperfine transition for $m = +\frac{1}{2}$, (b) the electronic hyperfine transition for $m = -\frac{1}{2}$. On this simple model, Endor transitions can be observed by applying nuclear power to the nuclear transitions between levels whose population differences are of order δ_e, i.e. to the upper nuclear transition $h\nu_n^+$ in (a) and the lower nuclear transition $h\nu_n^-$ in (b).

4.10(a) only between the nuclear levels for $M = +\frac{1}{2}$, and not between the nuclear levels for $M = -\frac{1}{2}$. Since application of nuclear power can only promote equalization of the populations of the two levels between which transitions are induced, it follows that an Endor signal will be observed only from the transition $h\nu_n^+$ in Fig. 4.10(a), and only from $h\nu_n^-$ in Fig. 4.10(b). (b) We consider the change in effective relaxation rate. In Fig. 4.9, saturation of the $h\nu_n^-$ transition instead of the $h\nu_n^+$ transition can only influence the return flow towards thermal equilibrium from the M, $m = +\frac{1}{2}, +\frac{1}{2}$ to the $-\frac{1}{2}, +\frac{1}{2}$ levels via the more indirect path

$$++ \xrightarrow{\tau_n} +- \xrightarrow{\tau_1} -- \xrightarrow{w_n} -+,$$

where the controlling rate will be the slowest relaxation rate $1/\tau_n$. Hence we can expect a fractional change in τ_1 only of order (τ_1/τ_n).

It is found in general that both Endor transitions can be observed (though often with unequal intensities) while saturating either hyperfine electronic line, showing that our model of the relaxation paths is

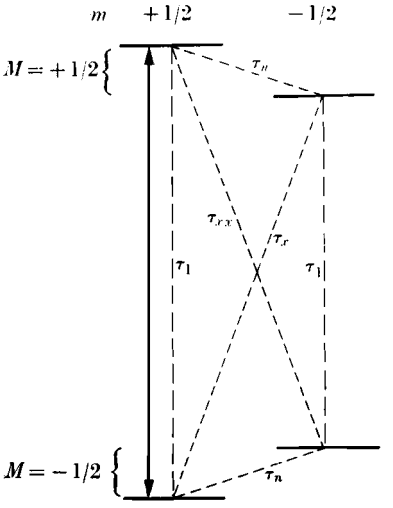

FIG. 4.11. Relaxation paths for a system $S = I = \frac{1}{2}$, with the spin Hamiltonian

$$\mathscr{H} = \beta(\mathbf{H} \,.\, \mathbf{g} \,.\, \mathbf{S}) + (\mathbf{S} \,.\, \mathbf{A} \,.\, \mathbf{I}).$$

The continuous vertical line represents the strong $(+\frac{1}{2}, +\frac{1}{2}) \leftrightarrow (-\frac{1}{2}, +\frac{1}{2})$ electron resonance transition. Relaxation via the path labelled τ_{xx} does not occur when the hyperfine interaction is isotropic. In general, $(1/\tau_1) \gg (1/\tau_x)$, $(1/\tau_{xx}) \gg (1/\tau_n)$.

over-simplified. We now consider a number of ways in which it can be modified.

When the magnetic hyperfine interaction is anisotropic, transitions between the $(+\frac{1}{2}, +\frac{1}{2})$ and $(-\frac{1}{2}, -\frac{1}{2})$ states are also partially allowed, and correspondingly there is an additional relaxation path labelled τ_{xx} in Fig. 4.11. When electron resonance power is applied to the $\Delta M = \pm 1$, $m = +\frac{1}{2}$ line, as shown in Fig. 4.11, spins are 'pumped' from the lower to the upper of these two states. In addition to the direct return flow through τ_1, there are additional return flows of the type

$$|++\rangle \xrightarrow[\tau_n]{} |+-\rangle \xrightarrow[\tau_x]{} |-+\rangle,$$
$$|++\rangle \xrightarrow[\tau_{xx}]{} |--\rangle \xrightarrow[\tau_n]{} |-+\rangle,$$

and

$$|++\rangle \xrightarrow[\tau_n]{} |+-\rangle \xrightarrow[\tau_1]{} |--\rangle \xrightarrow[\tau_n]{} |-+\rangle.$$

If the relaxation times are widely disparate, then the flow is controlled by the longest relaxation times, which are normally τ_n. If in the first two return paths, saturating power $(w_n\tau_x) > 1$ is applied at either of the nuclear frequencies, the effective value of τ_1 is altered by an amount of order (τ_1/τ_x) or (τ_1/τ_{xx}). It is true that if both nuclear

frequencies are applied simultaneously at saturating level, we can also get a change through the third path, but the need for two frequencies to be at the correct value obviously creates difficulties when searching for an unknown Endor frequency.

We can obtain an estimate of the relative orders of magnitude of the various relaxation times by assuming that

(a) relaxation takes place by a 'direct' process (see § 1.11 and Chapter 10), involving the absorption and emission of phonons at the magnetic resonance frequencies;

(b) the only important mechanism is the interaction between the electron spin and a thermal 'noise spectrum' producing oscillatory magnetic fields of magnitude $\sim h_1$ such that $|h_1|^2$ is isotropic in space, and independent of frequency at least over a band of order (A/h), which includes all the hyperfine transitions in the vicinity of the electron resonance frequency ν.

On this basis the relative relaxation rates for different electronic transitions vary in the same way as the transition probabilities in the magnetic resonance spectrum. The sloping relaxation paths τ_x, τ_{xx} arise through transitions partly allowed by the terms in the static spin Hamiltonian

$$A'_x S'_x I'_x + A'_y S'_y I'_y = \tfrac{1}{4}(A'_x + A'_y)(S'_+ I'_- + S'_- I'_+) + \tfrac{1}{4}(A'_x - A'_y)(S'_+ I'_+ + S'_- I'_-), \quad (4.31)$$

where the primes indicate that we have chosen coordinate systems for electron and nucleus such that the electronic Zeeman interaction and (as far as possible) the magnetic hyperfine interaction are diagonalized (cf. Chapter 3; for a typical example of such terms, see eqn (3.52)). These terms admix states $(M \pm 1, m \mp 1)$ and $(M \pm 1, m \pm 1)$ into (M, m), with amplitudes $\sim (A'_x + A'_y)/4h\nu_e$ and $(A'_x - A'_y)/4h\nu_e$ respectively. The transition probabilities are proportional to the squares of these amplitudes, giving

$$\frac{1}{\tau_x} \sim \frac{1}{\tau_1}\left(\frac{A'_x + A'_y}{4h\nu_e}\right)^2; \quad \frac{1}{\tau_{xx}} \sim \frac{1}{\tau_1}\left(\frac{A'_x - A'_y}{4h\nu_e}\right)^2. \quad (4.32)$$

Thus $(1/\tau_{xx})$ vanishes when the magnetic hyperfine interaction is isotropic, and in particular cases such that $A'_x = A'_y$. There is also a different dependence on electron resonance frequency for τ_1 and τ_x, τ_{xx}; for the direct process in a Kramers doublet $(1/\tau_1)$ varies as H^4 or $(h\nu_e)^4$ (see eqn (10.69)), and hence from (4.32) we would expect $1/\tau_x$, $1/\tau_{xx}$ to vary only as H^2.

In a more general spin Hamiltonian we may have terms of the form $S'_z I'_\pm$ which lend some electronic character to the $\Delta M = 0$, $\Delta m = \pm 1$ transitions. An effect of the same order of magnitude arises from the effect of a thermal low-frequency oscillatory field (normal to **H**) in driving the electronic magnetization, and hence producing an oscillatory component in the hyperfine field $\mathbf{H}_e$ at the nucleus (see § 4.3). These effects give matrix elements for the transitions $\Delta M = 0$ whose square is $(A/h\nu_e)^2 \times$the square of the matrix elements for the electronic transitions $\Delta m = 0$. However in estimating relaxation times we must also remember that the phonon density at the nuclear frequency ν_n is smaller by a factor $(\nu_n/\nu_e)^2$ than that at the electron frequency ν. Hence we expect

$$\frac{1}{\tau_n} \sim \frac{1}{\tau_x}\left(\frac{\nu_n}{\nu_e}\right)^2, \tag{4.33}$$

which is of order

$$\frac{1}{\tau_n} \sim \frac{1}{\tau_1}\left(\frac{A}{h\nu_e}\right)^4, \tag{4.34}$$

since $(h\nu_n/h\nu_e)^2 \sim (A/h\nu_e)^2$ and, from eqn (4.32), $(1/\tau_x) \sim (1/\tau_1)(A/h\nu_e)^2$.

In addition to the relaxation processes considered above, which may be regarded as by-products of the simple electron spin-lattice relaxation mechanism, there are others that arise from thermal modulation of the hyperfine terms. Thermal modulation of the magnetic hyperfine interaction (Abragam 1955) has been considered by Jeffries (1960), who shows that it may contribute to all the relaxation paths shown in Fig. 4.11. Hence τ_{xx} may be finite even when the static Hamiltonian contains only an isotropic magnetic hyperfine interaction, since the thermal vibrations distort the lattice and give rise to all terms of the type given in eqn (1.62). Contributions to τ_1^{-1}, τ_x^{-1} and τ_{xx}^{-1} may all be of the same order, and unlike those in eqn (4.32), do not depend on the states being admixed by the static Hamiltonian. Thus at high static fields, modulation of the hyperfine interaction may make a more important contribution to τ_x^{-1}, τ_{xx}^{-1} than that indicated by eqn (4.32); the same is likely to be true for τ_n^{-1}. When $I > \frac{1}{2}$, we may have a further contribution to τ_n^{-1} through thermal modulation of the nuclear electric quadrupole coupling, which will produce terms of all the types in eqn (3.40a), even though the static quadrupole tensor vanishes (as for a Kramers doublet in cubic symmetry). Such terms will produce relaxation paths corresponding to the transitions $\Delta M = 0$, $\Delta m = \pm 1$ and $\Delta M = 0$, $\Delta m = \pm 2$ (cf. § 3.9). Yet another mechanism arises through the effect

of hyperfine interaction in breaking time reversal symmetry in a Kramers doublet (cf. Fig. 10.9 and the reference given there).

We have so far assumed that the spin packet width is determined by a true spin-spin relaxation time τ_2. However the application of power at the electron resonance frequency will shorten the lifetime of the electron states, and we inquire now whether this will increase the effective width of the spin packet. As before, we use the macroscopic formulae to provide a convenient mode of analysis without implying that exact numerical interpretation is possible in practice. From eqn (2.51) the rate w_e at which electronic transitions are induced is (for spin $S = \frac{1}{2}$)

$$w_e = \frac{\pi}{2}\gamma^2 H_1^2 f(\omega), \tag{4.35}$$

where H_1 is the amplitude of the oscillatory field at the electron resonance frequency. For a narrow spin packet whose width is determined by a true relaxation time τ_2 we have, from eqn (2.65), at exact resonance

$$f(\omega) = 1/(\pi\,\Delta\omega) = \tau_2/\pi,$$

so that we can write

$$u_e = \tfrac{1}{2}\gamma^2 H_1^2 \tau_2. \tag{4.36}$$

We have seen from eqn (4.29) that the condition for optimum Endor signal is $\gamma^2 H_1^2 \tau_1 \tau_2 = 3$, in which case (4.36) becomes

$$2w_e\tau_1 = 3. \tag{4.37}$$

(Note that this is just the condition that makes the denominator in eqn (1.134) equal to 4, so that the electron 'spin temperature' for the transition in question is raised to roughly four times the lattice temperature.) The electronic transition rate w_e changes $1/\tau_2$ by an amount $\sim w_e$. Hence if $\tau_1 \gg \tau_2$ we can satisfy (4.37) without increasing the Endor line width, but if τ_1 is so short that it is the determining factor in the spin packet width ($\tau_2 = \tau_1$), partial saturation of the electron resonance line will increase the Endor line width.

We are now in a position to make some rough estimates of the signal strength at the nuclear frequency needed to give an Endor signal. The rate at which nuclear transitions are induced is given by eqn (4.19),

$$w_n = \frac{\pi}{2}\left(\frac{g_1^{(I)}\beta H_{1n}}{\hbar}\right)^2 \{I(I+1) - m(m\pm 1)\} f(\omega). \tag{4.19}$$

At the centre of a nuclear line the shape function

$$f(\omega) = 1/(\pi\Delta\omega) = 1/(2\pi^2\,\Delta\nu),$$

where $2\Delta\nu$ is the overall width of the nuclear line at half intensity. Hence at the centre, assuming $I = \frac{1}{2}$ for which

$$\{I(I+1)-m(m-1)\} = 1,$$

we have

$$w_n = \frac{\pi}{\Delta\nu}\left(\frac{g_1^{(I)}\beta H_{1n}}{h}\right)^2 \tag{4.38}$$

and to approach saturation of the nuclear transition we need

$$2w_n\tau_x \sim 1,$$

assuming τ_x to be the fastest relaxation time with which we have to compete.

In measurements on a ligand hyperfine structure there is little enhancement of the nuclear transition rate, and we may take $g_1^{(I)}$ to be roughly equal to g_I. If the nuclear signal strength is assumed to be $H_{1n} = 1$ G, and $\Delta\nu = 10$ kHz, we find for a proton or an ^{19}F ligand nucleus that

$$2w_n \sim 10^4\ \mathrm{s}^{-1}.$$

Thus this value of H_{1n} is sufficient to produce appreciable saturation of the nuclear transition only if $\tau_x \geqslant 10^{-4}$ s, which is appreciably longer than the value of $\tau_2 = 1/(\Delta\nu) \approx 10^{-5}$ s, assumed for the spin packet width.

In considering Endor on the nucleus of the paramagnetic ion itself we expect considerable enhancement of the nuclear transition rate from 'stirring' the hyperfine field, as discussed in § 4.3. If for simplicity we assume **H** to be along an axis of symmetry (the z-axis) so that $A_x = A_y = A_\perp$, we have first from eqn (4.32)

$$\frac{1}{\tau_x} \sim \frac{1}{\tau_1}\left(\frac{A_\perp}{2h\nu_e}\right)^2. \tag{4.39}$$

Second, from eqn (4.18) we must now replace $g_1^{(I)}\beta H_{1n}$ by $(M/H)A_\perp H_{1n}$ so that for $I = \frac{1}{2}$ we have, instead of (4.38),

$$w_n = \frac{\pi}{\Delta\nu}\left(\frac{MA_\perp H_{1n}}{hH}\right)^2, \tag{4.38a}$$

and since $h\nu_e = g_\parallel\beta H$ we find that in this case

$$2w_n\tau_x = \frac{2\pi\tau_1}{\Delta\nu}\left(\frac{2Mg_\parallel\beta H_{1n}}{h}\right)^2, \tag{4.40}$$

independent of both $A_\perp$ and of ν_e, except that τ_1 may vary with ν_e. If

we take $|M| = \frac{1}{2}$, $g_{\|} = 2$ and $H_{1n} = 10^{-2}$ G, $\Delta = 10$ kHz, we obtain

$$2w_n\tau_x \sim 5\times 10^5\tau_1,$$

so that even with this value of H_{1n} we can strongly saturate the nuclear transition provided that $\tau_1 \geqslant 10^{-5}$ s, a condition that must in any case be fulfilled if we are to keep the value of $\Delta\nu$ down to the region of 10 kHz.

In conclusion, we point out that saturation of the 'forbidden' transitions such as $\Delta(M+m) = 0$, which is a powerful tool in creating dynamic nuclear polarization (see § 1.12), is not an efficient method for Endor, since the nuclear transition rate w_n must then compete with the fastest relaxation rate $1/\tau_1$ in order to affect the intensity of the electronic transition that is being saturated.

4.7. The hyperfine structure of europium

As a second illustration of the power of the Endor technique we shall discuss the measurement of the hyperfine structure and nuclear moments of europium. The europium atom has the configuration $4f^76s^2$ and the dipositive ion Eu^{2+} has the configuration $4f^7$, so that both contain half-filled $4f$ shells and the ground spectroscopic state is ${}^8S_{\frac{7}{2}}$. The presence of the two extra electrons in the $6s$ shell of the atom makes little difference to the $4f$ electrons, but the magnetic hyperfine structure is distinctly larger in the ion. This difference is ascribed to core polarization, a conclusion that is supported by measurement of the hyperfine anomaly.

Europium has two stable isotopes, of mass 151 and 153, of roughly equal abundance. Each has nuclear spin $\frac{5}{2}$, but the nuclear magnetic dipole moments and nuclear electric quadrupole moments of the two isotopes each differ by a factor 2, though in opposite directions. The magnetic hyperfine anomaly is defined by the ratio

$$\frac{A(151)}{A(153)} = \frac{g_I(151)}{g_I(153)}(1+\Delta), \tag{4.41}$$

and Δ vanishes (see § 17.7) unless

(i) there is a finite density of magnetic electrons with a spatial variation within the nucleus (in practice this means that s-electrons must contribute to the magnetic hyperfine structure);

(ii) the nuclear magnetic dipole moment must be differently distributed within the nucleus for each isotope. (It was anticipated that this might be the case in view of the large differences in the nuclear moments quoted above.)

Obviously a hyperfine anomaly ($\Delta \neq 0$) can be observed only if the nuclear dipole moments and the magnetic hyperfine structure constants can be measured for both isotopes. This has been carried out for the ion by means of Endor in the solid state (Eu^{2+} in CaF_2), and for the atom by means of atomic beam triple resonance; nuclear magnetic resonance cannot be used to determine the nuclear moments because no configuration is available which does not have a resultant electronic angular momentum.

The atomic beam results for the atom are fitted to a Hamiltonian

$$\mathscr{H} = g\beta(\mathbf{H}\,.\,\mathbf{S}) - g_I\beta(\mathbf{H}\,.\,\mathbf{I}) + A(\mathbf{S}\,.\,\mathbf{I}) + \frac{B}{2I(2I-1)2S(2S-1)} \times \times \left[\begin{array}{r} \{3S_z^2 - S(S+1)\}\{3I_z^2 - I(I+1)\} + \tfrac{3}{2}(S_zS_+ + S_+S_z)(I_zI_- + I_-I_z) + \\ + \tfrac{3}{2}(S_zS_- + S_-S_z)(I_zI_+ + I_+I_z) + \tfrac{3}{2}(S_+^2I_-^2 + S_-^2I_+^2) \end{array} \right], \tag{4.42}$$

where the first two terms represent the Zeeman interactions, the third the magnetic hyperfine structure, and the last the electric quadrupole interaction. The same Hamiltonian is used for the ionic spectrum with some additional terms, which arise because of the cubic crystal field. These will be discussed in §§ 5.9, 5.10 and here we shall consider only the principal hyperfine terms.

The results of a number of measurements of the hyperfine constants are given in Table 4.2. We consider first the magnetic hyperfine interaction constant A. This may be regarded as a sum of contributions from

TABLE 4.2

Comparison of hyperfine measurements for the europium atom by atomic beam and for Eu^{2+} *in* CaF_2 *by Endor. In each case the ground state is* $4f^7$, ^8S, *and the data are based on the work of Sandars and Woodgate (1960), Evans, Sandars, and Woodgate (1965), and Baker and Williams (1962). The values of* g_I *are uncorrected for diamagnetism, and are expressed in Bohr magnetons (eqn (4.42)); the nuclear magnetic moments are positive*

	Eu atom	Eu^{2+} in CaF_2
g	1·9934(1)	1·9926(3)
^{151}A (MHz)	−20·0523(2)	−102·9069(13)
^{151}B (MHz)	−0·7012(35)	−0·7855(52)
$^{151}g_I$	$+7{\cdot}4921(13)\times10^{-4}$	$+7{\cdot}4969(20)\times10^{-4}$
$^{151}A/^{153}A$	+2·26498(8)	+2·25313(15)
$^{151}B/^{153}B$	+0·393(3)	+0·387(4)
$^{151}g_I/^{153}g_I$	+2·26505(42)	+2·2632(26)
Δ (%)	−0·003(20)	−0·53(2)

the $4f$ electrons, A_f, and from polarization of the core which we write as A_s because the dominant contribution must be from s-electrons through their finite density at the nucleus. Since only s-electrons are expected to contribute to the hyperfine anomaly, we can write, following Baker and Williams (1962),

$$A = A_f + A_s, \qquad A\Delta = A_s\Delta_s \tag{4.43}$$

where Δ is the measured anomaly and Δ_s that due to s-electrons. We have two pairs of such equations, one pair for the atom and one pair for the ion. In each pair there are three unknowns, A_f, A_s, and Δ_s but only two measured quantities, A and Δ, so that some further assumptions must be made to obtain a solution. These are: (1) that Δ_s is independent of the principal quantum numbers of the s-electrons involved (see Pichanick, Sandars, and Woodgate (1960)), so that Δ_s can be taken to be the same for atom and ion; (2) that A_f (ion) can be plausibly related to A_f (atom).

We consider first the atom, for which the measured anomaly (see Table 4.2) is essentially zero, showing that we must take $A_s(\text{atom}) = 0$. We have then the problem of accounting for the observed value of $A(\text{atom})$, which on this basis must arise from the f-electrons. For a pure ^8S state A_f should be zero, since there is no orbital moment and the spherical distribution of spin density gives no field at the nucleus, provided there is no core polarization. However it is well known that the spin-orbit coupling tends to break down LS-coupling, giving a ground state that is of the form

$$(1+\alpha^2)^{-\frac{1}{2}}\{|^8S_{\frac{7}{2}}\rangle + \alpha\,|^6P_{\frac{7}{2}}\rangle + \ldots\}.$$

The difference between the measured g-value and the spin-only value can be explained on this basis, but it turns out that the contributions to the hyperfine constants A, B are both positive (the best estimates are $+7{\cdot}70$ MHz for ^{151}A and $+1{\cdot}87$ MHz for ^{151}B). It was suggested by Sandars and Woodgate (1960) that the discrepancy might be due to relativistic contributions. The theory of these effects has been worked out by Sandars and Beck (1965), and for europium Evans, Sandars, and Woodgate (1965) estimate that they could account for about half the remaining discrepancy in A_f and nearly all that in B. It may be that calculations with better wave-functions could remove the discrepancy entirely, but the important point is that the relativistic effects give contributions of the right sign, and that they involve the $4f$ electrons (not s-electrons) and therefore give rise to no hyperfine anomaly.

Similar effects will be present in the ion, but in the absence of more precise calculations we probably cannot do better than assume that the value of A_f is the same for the ion as the measured value of A in the atom. We then obtain $^{151}A_s(\text{ion}) = -83$ MHz, $\Delta_s(\text{ion}) = -0{\cdot}66$ per cent, which agrees well with the best value from the optical spectrum of $\Delta_s = -0{\cdot}64(10)$ per cent deduced by Bordarier, Judd, and Klapisch (1965) from the measurements of Müller, Steudel, and Walther (1965).

The theory indicates that no anomaly is to be expected in the nuclear electric quadrupole interaction, so that the ratio of $B(151)/B(153)$ should be the same for atom and for ion; reference to Table 4.2 confirms that this prediction is fulfilled. However, as remarked above, the negative sign for B can only be explained by relativistic effects. For a pure ^8S state the electronic charge distribution is accurately spherical and no electric field gradient at the nucleus would be expected. The small break-down of LS-coupling which admixes $^6P_{\frac{7}{2}}$, etc., would give a positive value of B, estimated as $+1{\cdot}87$ MHz for the isotope 151 (Evans, Sandars, and Woodgate 1965), but these authors find that relativistic effects contribute an amount $-2{\cdot}44$ MHz, giving a total of $-0{\cdot}57$ MHz in reasonable agreement with the experimental value of $-0{\cdot}70$ MHz for the atom. Similar contributions would be expected in the ion, and it is reassuring to find that the observed value of $-0{\cdot}78$ MHz is reasonably close to that for the atom.

We have described the results of Endor measurements on Eu^{2+} ions in CaF_2, and of atomic beam triple resonance measurements on the Eu atom, in some detail because they illustrate the following points.

(a) They confirm that most of the contribution to the isotropic magnetic hyperfine constant in the ion comes from core polarization, though relativistic effects are not negligible (and may be expected to be increasingly important in heavier ions);

(b) they show that Endor measurements of hyperfine constants can be made with an accuracy approaching that of magnetic resonance experiments on atoms using conventional atomic beam methods;

(c) they give measurements of the nuclear Zeeman interaction with an accuracy comparable with atomic beam triple resonance experiments.

The latter does not always mean that the nuclear magnetic moment can be determined with comparable accuracy. Both in atoms and in ions there may be an appreciable pseudo-nuclear Zeeman interaction, but this can generally be calculated more accurately for atoms because

more exact information on excited states is available, in particular because crystal field interactions are absent. Obviously ions with half-filled shells are exceptional in this respect, and in the following section we discuss another type of ion where the interpretation of the Endor results involves a number of correction terms.

4.8. The Endor spectrum of Nd^{3+} in $LaCl_3$

We consider now the Endor spectrum of an ion where a number of important corrections must be included in the hyperfine structure owing to the presence of nearby excited electronic states. This ion is Nd^{3+}, $4f^3$, whose Endor spectrum has been analyzed very fully by Halford (1962). The ground state of this ion, which has $L = 6$, $S = \frac{3}{2}$, is $J = \frac{9}{2}$, which is split by the crystal field (see § 5.6) into five doublets. Resonance is observed in the lowest of these, and fitted to a spin Hamiltonian of the usual form for effective spin $S = \frac{1}{2}$ and axial symmetry

$$\begin{aligned}\mathscr{H} = {} & g_{\parallel}\beta H_z S_z + g_{\perp}\beta(H_x S_x + H_y S_y) + \\ & + A'_{\parallel} S_z I_z + A_{\perp}(S_x I_x + S_y I_y) + \\ & + P'_{\parallel}\{I_z^2 - \tfrac{1}{3}I(I+1)\} - \\ & - g_{\parallel}^{(n)}\beta_n H_z I_z - g_{\perp}^{(n)}\beta_n(H_x I_x + H_y I_y). \end{aligned} \tag{4.44}$$

This is essentially the same as discussed in Chapter 3 except that primed coefficients have been used for $A'_{\parallel}$ and $P'_{\parallel}$ to denote the presence of correction terms, and the nuclear g-factor (here expressed in terms of nuclear magnetons) is allowed to be anisotropic because of contributions from the pseudo-nuclear Zeeman effect.

The electronic g-factor was determined from measurements on the single strong line in the electron spin resonance spectrum due to the even isotopes of Nd, the values obtained being

$$g_{\parallel} = +3{\cdot}9903(5), \qquad |g_{\perp}| = 1{\cdot}7635(12). \tag{4.45}$$

A large number of Endor measurements were made for the two odd isotopes ^{143}Nd, ^{145}Nd, each of which has $I = \frac{7}{2}$, and fitted by a least squares procedure using computer diagonalization of the Hamiltonian; the more accurate sets of results are shown in Table 4.3. The values of $A'_{\parallel}$ and $P'_{\parallel}$ determined with the magnetic field along the crystal axis are the more accurate, and were used in the subsequent analysis. As pointed out in § 4.2, the relative signs of $g_{\parallel}$ and $g_{\parallel}^{(n)}$, and of $A'_{\parallel}$ and $P'_{\parallel}$, can be determined from the Endor experiments. The crystal field analysis shows $g_{\parallel}$ to be positive, and that the sign of $A'_{\parallel}$ is the same as

TABLE 4.3

Results of Endor measurements on Nd^{3+} *in* $LaCl_3$ *(from Halford (1962)). Column 2 gives the orientation of the external magnetic field* **H** *relative to the crystal axis*

Isotope	H	$A'_{\parallel}$ (MHz)	$\lvert A_{\perp}\rvert$ (MHz)	$P'_{\parallel}$ (MHz)	$g_{\parallel}^{(n)}$	$\lvert g_{\perp}^{(n)}\rvert$
^{143}Nd	$\parallel$	−1272·1428(80)	499·568(42)	+0·0887(10)	−0·543(3)	
	$\perp$	−1273·036(240)	499·532(40)	+0·136(15)		0·874(7)
^{145}Nd	$\parallel$	−790·736(16)	310·682(140)	+0·0427(22)	−0·347(18)	
	$\perp$	−790·810(300)	310·540(48)	+0·035(12)		0·538(9)

that of g_n, thus establishing the signs given in the table, but only after a complete analysis has been used to relate $g_{\parallel}^{(n)}$ to g_n.

To make full use of the high experimental accuracy a rather extensive crystal field analysis is required to determine accurately the wave functions $|+\rangle$ and $|-\rangle$ spanning the ground doublet, together with an approximate determination of the energies of the excited levels. This was carried out by Halford including contributions from the $J = \frac{11}{2}$ and $\frac{13}{2}$ manifolds (those from $J = \frac{15}{2}$ were shown to be negligible) as well as the first-order contributions from $J = \frac{9}{2}$, and including corrections due to intermediate coupling, from a fit to the optical spectrum by Judd (1959*a*). The results were checked against the experimentally determined electronic g-values of the ground doublet, and a small correction made.

To proceed further, we write out the parameters of the experimental spin Hamiltonian in some detail, separating out the correction terms. This gives

$$\left.\begin{aligned} A'_{\parallel} &= 4g_n\beta\beta_n\langle r^{-3}\rangle\langle +|\, N_z\,|+\rangle + C + \Delta A_{\parallel} \\ A_{\perp} &= 4g_n\beta\beta_n\langle r^{-3}\rangle\langle +|\, N_x\,|-\rangle + C \end{aligned}\right\} \tag{4.46}$$

$$P'_{\parallel} = -\frac{3e^2Q}{4I(2I-1)}\langle r^{-3}\rangle\langle +|\, M\,|+\rangle + \Delta P_{\parallel} \tag{4.47}$$

$$\left.\begin{aligned} g_{\parallel}^{(n)} &= g_n + \Delta g_{\parallel}^{(n)} \\ g_{\perp}^{(n)} &= g_n + \Delta g_{\perp}^{(n)} \end{aligned}\right\}. \tag{4.48}$$

In eqns (4.46) the first term is the first-order magnetic hyperfine parameter; **N** is the operator defined in eqn (17.48), and an extra factor 2 appears because the parameters $A_{\parallel}$, $A_{\perp}$ refer to the effective spin Hamiltonian (4.44) for which $\langle +|\, S_z\,|+\rangle = \frac{1}{2}$. The term C was introduced by Halford to allow for a possible contact hyperfine interaction

from unpaired s-electrons which he incorrectly assumed (see below) would give an isotropic contribution to the magnetic hyperfine structure. The extra term $\Delta A_{\parallel}$ is the second-order correction to the magnetic hyperfine structure given by eqn (18.9),

$$\Delta A_{\parallel} = -2u_{33} = -2d_3^{12},$$

which can be written according to eqn (18.8) for axial symmetry as

$$\Delta A_{\parallel} = 2(2g_{\mathrm{n}}\beta\beta_{\mathrm{n}}\langle r^{-3}\rangle)^2 \sum_n{}' \frac{\langle +|\, N_x\,|n\rangle\langle n|\, -iN_y\,|+\rangle}{W_0 - W_{\mathrm{n}}}. \tag{4.49}$$

It is readily verified that the corresponding correction $\Delta A_{\perp}$ which would involve terms

$$\frac{\langle +|\, N_x\,|n\rangle\langle n|\, N_z\,|-\rangle}{W_0 - W_{\mathrm{n}}} \tag{4.50}$$

vanishes and for that reason was omitted.

The quadrupole interaction (4.47) can be written as

$$P'_{\parallel} = P_{\parallel} + \Delta P_{\parallel}, \tag{4.51}$$

where $P_{\parallel}$ is the true quadrupole interaction, here assumed to arise only from the $4f$ electrons. In fact matrix elements between states of different J can be neglected, and the value of the matrix element is then

$$\langle +|\, M\,|+\rangle = \sum_J n_J^2\, \langle J\|\, \alpha\, \|J\rangle\langle +|3J_z^2 - J(J+1)\,|+\rangle, \tag{4.52}$$

where each term in the summation is weighted by n_J^2, the square of its amplitude in the ground state wavefunction.

The extra term $\Delta P_{\parallel}$ is the pseudo-quadrupolar interaction constant which, from eqn (18.8), can be written in the case of axial symmetry as

$$\Delta P_{\parallel} = \tfrac{3}{2}(2g_{\mathrm{n}}\beta\beta_{\mathrm{n}}\langle r^{-3}\rangle)^2 \sum_n{}' \frac{\langle +|\, N_z\,|n\rangle^2}{W_0 - W_{\mathrm{n}}}. \tag{4.53}$$

Both $\Delta A_{\parallel}$ and $\Delta P_{\parallel}$ are second-order effects of the magnetic hyperfine interaction, which admixes excited crystal field states into the ground states and thus changes (in second order) the hyperfine interactions.

Finally, $\Delta g_{\parallel}^{(\mathrm{n})}$ and $\Delta g_{\perp}^{(\mathrm{n})}$ are constants representing the pseudo-nuclear Zeeman effect whose values are, from eqn (18.2),

$$\left.\begin{aligned} \Delta g_{\parallel}^{(\mathrm{n})} &= -4g_{\mathrm{n}}\beta^2\langle r^{-3}\rangle \sum_n{}' \frac{\langle +|\, L_z + g_s S_z\,|n\rangle\langle n|\, N_z\,|+\rangle}{W_0 - W_{\mathrm{n}}}, \\ \Delta g_{\perp}^{(\mathrm{n})} &= -4g_{\mathrm{n}}\beta^2\langle r^{-3}\rangle \sum_n{}' \frac{\langle +|\, L_x + g_s S_x\,|n\rangle\langle n|\, N_x\,|+\rangle}{W_0 - W_{\mathrm{n}}}. \end{aligned}\right\} \tag{4.54}$$

Their interpretation is as follows: the electronic Zeeman interaction mixes excited crystal field states into the ground states and thus changes the magnetic hyperfine interaction by an amount proportional to the external magnetic field.

The value calculated for $\Delta A_{\parallel}$ is very small, being $+0{\cdot}0351(10)$ MHz for isotope 143, and $+0{\cdot}0136(4)$ MHz for isotope 145. The value of C can be found by comparing the ratio of $A'_{\parallel}-\Delta A_{\parallel}$ to $A_{\perp}$ found experimentally with that calculated for the ratio of $A_{\parallel}$ to $A_{\perp}$ from the crystal field states. C is found to be zero within the experimental error, but this does not imply that there is no core polarization effect. The matrix elements describing this effect are proportional to those of the vector $\mathbf{S}$; if the ground state wave-functions are accurately described by states belonging only to one manifold of given $\mathbf{J}$, the matrix elements both of $\mathbf{S}$ and of the Zeeman interaction $\mathbf{L}+g_s\mathbf{S}$ are each proportional to those of $\mathbf{J}$, and a core polarization contribution will not change the ratio $A_{\parallel}/A_{\perp}$. In so far as we cannot neglect admixtures from states of different $\mathbf{J}$, this proportionality will break down, and the ratio $A_{\parallel}/A_{\perp}$ will be affected, though the change cannot be represented by adding an isotropic contribution C. Since such admixtures in the present case are fairly small, and the expected contribution to the magnetic hyperfine structure from core polarization is probably only about 2 per cent (Bleaney (1964*b*)), the net effect is likely to be quite small.

We now consider the nuclear g-factors. The fact that $g_{\parallel}^{(n)}$ and $g_{\perp}^{(n)}$ are experimentally found to be quite different shows at once that the pseudo-nuclear Zeeman effect, which can be anisotropic, is playing an important role. In fact Halford's analysis gives $\Delta g_{\parallel}^{(n)} = -0{\cdot}235(18)$, $\Delta g_{\perp}^{(n)} = -0{\cdot}564(18)$ for isotope 143 which are of the same order as the value obtained for $g_n = -0{\cdot}308(18)$. The latter gives a nuclear magnetic moment of $-1{\cdot}079(60)$ n.m., in good agreement with the later result of Smith and Unsworth (1965) of $-1{\cdot}063(5)$ n.m., obtained from atomic beam triple resonance measurements on the free atom.

Halford's results also yield the values:

$$\left.\begin{array}{lll} \text{isotope 143} & \Delta P_{\parallel} = +0{\cdot}0302(8)\,\text{MHz}; & P_{\parallel} = +0{\cdot}0585\ \text{MHz} \\ \text{isotope 145} & \Delta P_{\parallel} = +0{\cdot}0117(3)\,\text{MHz}; & P_{\parallel} = +0{\cdot}0310\ \text{MHz} \end{array}\right\} \tag{4.55}$$

where only the more accurate values of $P'_{\parallel}$ obtained from measurements with the magnetic field parallel to the crystal axis are used to find $P_{\parallel}$. The latter is the true quadrupole interaction, and its ratio for the two

isotopes is 1·90, in very close agreement with the ratio of the quadrupole interaction constants for the free atom (Spalding (1963)). The pseudo-quadrupole effect $\Delta P_{\|}$ is of considerable importance, and since it is proportional to the square of the magnetic hyperfine constant and not to the quadrupole moment, the ratio of the constants $P'_{\|}$ for the two isotopes is quite different from that of the constants $P_{\|}$, which should also be the ratio of the quadrupole moments. The values of the quadrupole moments themselves, deduced by Halford are, however, quite different from those obtained from atomic beam measurements on the free atom, as follows:

	Halford (Nd^{3+} in $LaCl_3$)	*Smith and Unsworth* (Nd)
isotope 143	$Q = +0{\cdot}0206(30)$ barns	$Q = -0{\cdot}484(20)$ barns,
isotope 145	$Q = +0{\cdot}0105(20)$ barns	$Q = -0{\cdot}253(10)$ barns.

In each case a value of $\langle r^{-3} \rangle$ deduced from the magnetic hyperfine constant and the nuclear moment is used, but that for the atom is only a few per cent larger than that for the ion, as would be expected. We must therefore look elsewhere for an explanation of the discrepancy. Bleaney (1964*b*) has suggested that there is an appreciable contribution to $P_{\|}$ from the lattice, which, from the results of Edmonds (1963), might well be of the order of +1 MHz for isotope 143. From the atomic beam results we would expect the contribution from the 4*f* electrons for this isotope to be about −1·4 MHz in Halford's experiment, so that his value of $P_{\|} = +0{\cdot}06$ MHz could be explained if the lattice contribution were just over +1·4 MHz.

As discussed in § 5.5, the lattice contribution is enhanced by a large anti-shielding factor, while that of the 4*f* electrons is slightly diminished by shielding. In the compound used by Halford, the ground state wave-functions give an unusually small electric field gradient from the 4*f* electrons; in other cases the 4*f* electrons generally provide the dominant contribution to the electric field gradient. Nevertheless, the complications introduced by the crystal field make it unlikely that nuclear moment determinations by the Endor method in the solid state will approach in accuracy (except for ions with half-filled shells) those given by atomic beam methods for the free atoms of the 4*f* group.

4.9. Endor measurements of ligand hyperfine structure

Magnetic hyperfine structure due to interaction of the magnetic electrons with the nuclear magnetic moments of ligand ions is usually

fairly small, particularly in the rare-earth group, and it can be measured only with limited accuracy in e.s.r. experiments. A further disadvantage of such experiments is that the allowed transitions are usually those in which the ligand nuclear magnetic quantum number does not change, so that no measure of any electric quadrupole interaction (such as may exist if the ligand ions are chlorine, with $I = \frac{3}{2}$) is obtained. If transitions violating this selection rule are observed, the hyperfine pattern is usually so complicated that accurate measurements are very difficult. This is just the situation in which the Endor technique can be used to good advantage, and as an example we shall discuss measurements of the fluorine hyperfine structure in the Eu^{2+} spectrum in CaF_2 (Baker and Hurrell (1963)).

The crystal structure of CaF_2 is outlined in § 5.1; the point symmetry of the Eu^{2+} ion (substituting for Ca^{2+}) is cubic O_h, while that of the nearest neighbour fluorine is trigonal C_{3v} about its bond axis (the line joining it to the Eu^{2+} ion), which is a $\langle 111 \rangle$ axis of the crystal. This symmetry restricts the form of the magnetic hyperfine interaction to

$$A_{\parallel} S_{z'} I_{z'} + A_{\perp} (S_{x'} I_{x'} + S_{y'} I_{y'}), \tag{4.56}$$

where the z'-axis lies along the bond direction. Using the substitutions

$$A_{\parallel} = A_s + 2A_p \quad \text{and} \quad A_{\perp} = A_s - A_p \tag{4.57}$$

this can be resolved into an isotropic term and one that has the same form as the point dipolar interaction. The complete spin Hamiltonian for each nearest-neighbour fluorine nucleus is then

$$\mathscr{H}_{\mathrm{F}} = -g_I \beta \mathbf{H} \cdot \mathbf{I} + A_s \mathbf{S} \cdot \mathbf{I} + A_p (3 S_{z'} I_{z'} - \mathbf{S} \cdot \mathbf{I}), \tag{4.58}$$

where the z'-axis is along the appropriate bond axis and there are altogether eight such terms (with different bond axes, except that pairs of fluorine ions have the same bond axis because of the inversion symmetry about the Eu^{2+} site). The electronic Zeeman term is so large that to a good approximation off-diagonal terms in $\mathbf{S}$ can be neglected, and if $\mathbf{H}$ is applied along an axis (the z-axis) which makes an angle θ with the z'-axis, the relevant terms in the Hamiltonian are

$$\mathscr{H}_{\mathrm{F}} = -g_I \beta H I_z + A_s S_z I_z + A_p (3 \cos^2\theta - 1) S_z I_z + 3A_p \sin\theta \cos\theta S_z I_x, \tag{4.59}$$

which can be diagonalized (cf. § 3.11) by choosing a z_{n}-axis for the nuclear coordinates which makes an angle ϕ with the z-axis, such that

$$\tan\phi = \frac{3A_p \sin\theta \cos\theta}{-g_I \beta H + \{A_s + A_p (3\cos^2\theta - 1)\} S_z}. \tag{4.60}$$

The energy then has the values $\pm\frac{1}{2}h\nu_F$, and the nuclear transition $\Delta I_z = \pm 1$ between these two states occurs at frequency ν_F where

$$h\nu_F = [\{-g_I\beta H + A_s S_z + (3\cos^2\theta - 1)A_p S_z\}^2 + 9\sin^2\theta\cos^2\theta A_p^2 S_z^2]^{\frac{1}{2}}. \tag{4.61}$$

Essentially this formula reflects the fact that the nuclear transition takes place in a net magnetic field which is the vectorial sum of the external magnetic field and the steady component of the local magnetic field due to the magnetic electrons; the terms that have been neglected correspond to the rapidly precessing components of the electronic magnetic field to which the fluorine magnetic moment cannot in a first approximation react, owing to its gyromagnetic properties. The steady magnetic field of the magnetic electrons has components both parallel and perpendicular to the external magnetic field which are each proportional to the value of S_z. As a result, the nuclear frequency given by eqn (4.61) has terms involving the zero, first, and second power of S_z, and by making Endor measurements on different electronic lines there is more than enough information to determine all the terms separately even while working only at one particular value of θ.

In practice all accurate measurements of the Endor transitions were made with **H** along a $\langle 100\rangle$ direction where all eight nearest neighbour fluorines are equivalent with $\cos^2\theta = \frac{1}{3}$. Other measurements to confirm the sign of the interactions and the general form of eqn (4.58) were made in a $\langle 110\rangle$ direction where four nearest neighbours have $\cos^2\theta = 0$ and four have $\cos^2\theta = \frac{2}{3}$. The advantages of such directions were: (i) the e.s.r. spectrum of eighty-four lines was almost resolved so that the line being saturated can be identified; (ii) the fluorine Endor spectrum is greatly simplified owing to the high degeneracy; (iii) this degeneracy enabled the crystal to be accurately aligned using the Endor spectrum.

Using a value of $H_1 \approx 0{\cdot}1$ G for the nuclear driving field, the relative intensities of different nearest-neighbour transitions were found to vary by a factor of about 50, with a best signal/noise ratio of $\sim$60 for a time constant of 1 s. The average line width was about 40 kHz with no resolved splitting, and this width could be explained by the accuracy of about 0·1° in orienting the crystal. An analysis of thirty-seven lines gave

$$A_s = -2{\cdot}23(1)\text{ MHz}, \quad A_p = +4{\cdot}01(1)\text{ MHz}; \quad \text{(nearest neighbours)}.$$

The sign of A_p cannot be found from measurements in a $\langle 100\rangle$ direction, since $(3\cos^2\theta - 1)$ is then zero, but is found relative to that of g_I from

measurements in a ⟨110⟩ direction. Likewise the sign of A_s is obtained only relative to that of g_I, but the latter is known to be positive. These sign determinations are possible because $S > \frac{1}{2}$ and the signs of S_z are known, through the methods described in Chapter 3. The value of A_p is somewhat smaller than the value of +5·7 MHz calculated for point dipoles, and suggests that some bonding occurs, since the alternative explanation of a reduction of 10 per cent in the bond length when Eu^{2+} is substituted for Ca^{2+} seems unlikely.

The analysis of twenty-eight next nearest neighbour lines gave $A_s = -7(5)$ kHz, $A_p = +785(5)$ kHz; (next nearest neighbours) which is consistent within the accuracy of the measurement and first-order theory with a purely point dipole interaction, for which

$$A_s = 0;\ A_p = A_d = +0{\cdot}8\ \text{MHz}.$$

Endor measurements have also been made of the fluorine hyperfine interaction for two ions with the configuration $4f^{13}$ in CaF_2; these are Tm^{2+} (Bessent and Hayes 1965) and Yb^{3+} (Ranon and Hyde 1966). In each case the ion has cubic symmetry, and the ground state is a

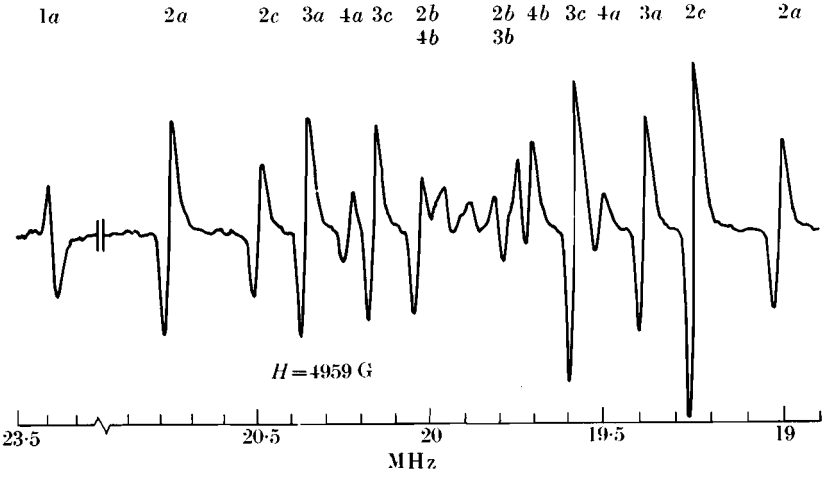

FIG. 4.12. Fluorine Endor spectrum for Tm^{2+} in CaF_2. The electron paramagnetic resonance is observed at about 24000 MHz and H = 5000 G, directed along the ⟨111⟩ axis, using magnetic field modulation at 115 kHz, giving an output after detection at this frequency. This output varies as a nuclear resonance oscillator (modulated at ~100 Hz) is swept through the Endor spectrum. After detection, the 115-kHz signal is amplified and passed to a synchronous detector at the second modulation frequency, whose output feeds (through a smoothing circuit with a 10 s time-constant) a chart recorder. The ordinate represents $\delta^2\chi''/\delta\nu\,\delta H$, the derivative with respect to frequency of the derivative $\delta\chi'/\delta H$ of the e.p.r. dispersion line. The lines labelled 1, 2, 3, 4 arise from fluorines in the first, second, third, and fourth shells. (After Bessent and Hayes 1965.)

Γ_7 doublet with an isotropic g-factor close to 3·45. A typical Endor spectrum is shown in Fig. 4.12 and the results are summarized in Table 4.4. For Tm^{2+}, as for Eu^{2+}, the interaction with more distant shells of fluorines is found to agree within experimental error with that

TABLE 4.4

Endor measurements of the fluorine hyperfine interaction of some rare-earth ions in CaF_2. *The actual signs are experimentally determined only for* Eu^{2+}, *but for the other ions* (A_s/A_p) *is found to be positive.* A_s, A_p *are the parameters in the effective spin Hamiltonian (eqn (4.58));* A_d *is the value that* A_p *would have (with* $A_s = 0$) *if the interaction were that between two point dipoles situated in an undistorted* CaF_2 *lattice*

		Nearest fluorine neighbours			Second nearest fluorine neighbours			
		A_s (MHz)	A_p (MHz)	A_d (MHz)	A_s (MHz)	A_p (MHz)	A_d (MHz)	Reference
$4f^7$	Eu^{2+}	−2·23(1)	+4·01(1)	+5·7	−0·007(5)	+0·785	+0·81	Baker and Hurrell (1963)
$4f^{13}$	Tm^{2+}	2·584(10)	12·283(10)	+9·8	0·010(10)	1·386(5)	+1·40	Bessent and Hayes (1965)
$4f^{13}$	Yb^{3+}	1·67(5)	17·57(5)	+9·8				Ranon and Hyde (1966)

expected for a point dipole interaction; this is larger for Tm^{2+} than for Eu^{2+} in the ratio of the electronic g-values 3·45:2·00. The interaction with the nearest-neighbour fluorines is not point dipole, nor is it purely dipolar in character, since some s-character is found. The sign of the interaction is not determined for the $4f^{13}$ ions where the electronic ground state is a doublet, but is assumed to be positive for both A_s and A_p (experimentally these are found to have the *same* sign), since otherwise the difference between A_p and the point dipole value A_d appears to be implausibly large.

To make a proper comparison of the non-dipolar part of the interaction for the different ions we must allow for the fact that the interaction for the $4f^{13}$ ions is expressed in terms of the effective spin of $\frac{1}{2}$ for the electronic state, which is not the same as the true spin. The

Γ_7 doublet states are (neglecting any admixture of $J = \frac{5}{2}$ into $J = \frac{7}{2}$)

$$|\pm\rangle = \pm\sqrt{(\tfrac{3}{4})}\,|J_z = \pm\tfrac{5}{2}\rangle\mp\tfrac{1}{2}\,|J_z = \mp\tfrac{3}{2}\rangle \tag{4.62}$$

$$= \pm\sqrt{(\tfrac{3}{4})}\{\sqrt{(\tfrac{6}{7})}\,|\pm 2,\ \pm\rangle + \sqrt{(\tfrac{1}{7})}\,|\pm 3,\ \mp\rangle\}\mp \mp\tfrac{1}{2}\{\sqrt{(\tfrac{5}{7})}\,|\mp 1,\ \mp\rangle + \sqrt{(\tfrac{2}{7})}\,|\mp 2,\ \pm\rangle\}, \tag{4.63}$$

where the last representation is in terms of $|l_z, s_z\rangle$. From this it can be verified that the expectation values of the true spin component s_z are $\pm\frac{3}{14}$ in the two doublet states, and are thus a factor $(\frac{3}{7})$ smaller than the expectation values of the effective spin. Thus the non-point dipole parts, A_s and $(A_p - A_d)$, of the hyperfine interaction for the $4f^{13}$ ions must be increased by a factor $(\frac{7}{3})$ for comparison with Eu^{2+}. With this change one finds that the isotropic interaction is larger for both the $4f^{13}$ ions than for Eu^{2+}; so also is the adjusted value of $A_p - A_d$. The signs are also probably different for A_s, as well as for $A_p - A_d$; (if the signs of A_s are assumed to be all negative, the resultant value of $A_p - A_d$ becomes an order of magnitude larger for the $4f^{13}$ ions than for Eu^{2+}, though of the same sign). The rather larger value of A_p for Yb^{3+} compared with Tm^{2+} (both assumed positive) could be partly due to a larger point dipole interaction if the extra charge on the former ion pulls the nearest F^- ions inwards by an appreciable amount.

The ligand hyperfine interaction discussed in this section and in § 4.10 is not essentially different from the interaction between the nuclear moments of ^{29}Si in the host lattice and the donor electron in silicon (§ 4.4), as can be seen from a comparison of eqns (4.22) and (4.58). If the magnetic electrons were wholly localized on the parent ion (or donor), interaction with a ligand nucleus would be purely 'point dipole', i.e. the same as that for two magnetic point dipoles. The additional ligand interaction comes from delocalization of the magnetic electrons. In silicon their wave-function spreads widely, and the resultant hyperfine interaction does not decrease monotonically with distance. In the $4f$ group bonding takes place only to the immediate ligand ions, and the degree of electron transfer is usually small. In the $3d$ group the transfer is usually larger, and may not be confined to the immediate ligand neighbours.

4.10. Endor line widths

To obtain narrow Endor lines the value of τ_2, the true spin-spin relaxation time, must be fairly long and in most cases this means that the main cause of broadening of the electron paramagnetic resonance line must be inhomogeneous. Then ideally one spin packet of width

$\Delta\omega \sim 1/\tau_2$ is saturated at the centre of the electron hyperfine transition $(M, m) \leftrightarrow (M-1, m)$, and only spins within this packet take part in the Endor transitions $(M, m) \leftrightarrow (M, m \pm 1)$, $(M-1, m) \leftrightarrow (M-1, m \pm 1)$. If $\tau_2 \sim 10^{-5}$ s, then the Endor line width parameter $\Delta\nu_n = 1/(2\pi\tau_2)$ should be of order 10 kHz. In practice the ideal situation is not always attained, and we now consider three reasons for this: inhomogeneous broadening, cross-relaxation within the electron spin system, and spin diffusion within the nuclear spin system.

Inhomogeneous broadening

When the effective spin $S \geqslant 1$ it is frequently observed that the electronic transitions are broadened owing to random variations in the crystal field from site to site. The electron resonance energy may be written

$$h\nu_e = g\beta H + g\beta\Delta H + (h\nu_e)_{fs} + (h\nu_e)_{hfs} + \tag{4.64}$$

$$+ \delta g\beta H + \delta(h\nu_e)_{fs} + \delta(h\nu_e)_{hfs}, \tag{4.65}$$

where ΔH is the random variation of local field due to magnetic dipole moments of neighbouring ions or nuclei. The terms $(h\nu_e)_{fs}$ and $(h\nu_e)_{hfs}$ represent the energy contributions from fine structure terms or 'initial splittings' (see §§ 3.3 to 3.6) and hyperfine terms respectively. The terms $\delta g\beta H$, $\delta(h\nu_e)_{fs}$ and $\delta(h\nu_e)_{hfs}$ represent respectively the effect of random variation in the crystal field giving rise to random variations in g, and in the fine structure and hyperfine structure contributions. The first of these may always occur, but the second is present only for $S \geqslant 1$. As discussed in § 3.13, for $S \geqslant \frac{3}{2}$ it is manifested in the electron resonance spectrum by a narrower line width for the $M = +\frac{1}{2} \leftrightarrow -\frac{1}{2}$ transition than for the outer transitions, since changes in the fine structure parameters affect the position of the central transition only in second order but the others in first order.

If random crystal field effects are absent, a fixed value of ν_e and a fixed value of H allow the resonance condition to be satisfied only for one value of ΔH. If, on the other hand, random crystal fields do contribute to the line width, then even for fixed ν_e and H, the term $g\beta\Delta H$ and those in (4.65) can vary at random so long as their sum is constant. However the terms in (4.65) do not necessarily vary independently of one another, as has been elegantly demonstrated by an Endor experiment of Locher and Geschwind (1963) on ^{61}Ni ($I = \frac{3}{2}$) in Al_2O_3, where the Ni^{2+} ion has an effective spin $S = 1$. The ion has axial symmetry about the z-axis, and for a magnetic field directed along this

axis the diagonal parts of the spin Hamiltonian are

$$\mathscr{H} = g_{\parallel}\beta H S_z + D\{S_z^2 - \tfrac{1}{3}S(S+1)\} + \\ + A_{\parallel} S_z I_z + P_{\parallel}\{I_z^2 - \tfrac{1}{3}I(I+1)\} - g_{\parallel}^{(I)}\beta H I_z. \qquad (4.66)$$

The electron resonance condition for the transition $(M, m) \leftrightarrow (M-1, m)$ is

$$h\nu_e = |g_{\parallel}\beta H + D(2M-1) + A_{\parallel} m|, \qquad (4.67)$$

from which it is clear that a variation δD in D due to random crystal field effects must be compensated by a variation in H that will be of opposite sign for the two allowed transitions for which $(2M-1)$ has the values $+1$ and -1 respectively. Thus points within the electron

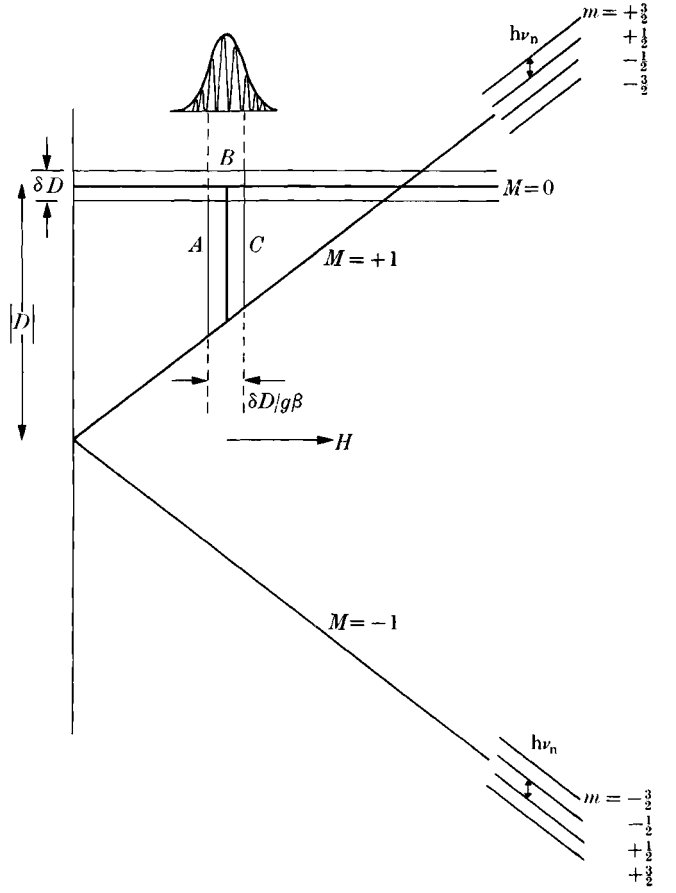

FIG. 4.13. Effect of inhomogeneity in the value of D for an ion such as Ni^{2+} ($S = 1$) in Al_2O_3, with the spin Hamiltonian of eqn (4.66). The Endor transitions of energy $h\nu_n$ shown are for the isotope ^{61}Ni ($I = \frac{3}{2}$). (After Locher and Geschwind 1963.)

resonance line associated with different values of H correspond to different values of D, as illustrated in Fig. 4.13.

The Endor transition $(M, m) \leftrightarrow (M, m-1)$ requires a quantum

$$h\nu_n = |A_\parallel M + P_\parallel(2m-1) - g_\parallel^{(I)}\beta H| \tag{4.68}$$

and, in principle, the values of $A_\parallel$ and $P_\parallel$, and also of $g_\parallel^{(I)}$ if it contains an appreciable 'pseudo-nuclear Zeeman' contribution, may all vary in a manner linked to the crystal field, and hence to the value of D. In fact only the variation in $A_\parallel$ is significant in this case, and Locher and Geschwind showed that as H was varied through the resonance lines the value of $h\nu_n$ varied linearly not just as $-g^{(I)}\beta H$ but as

$$\delta(h\nu_n) = |(\delta A_\parallel/\delta H)M - g_\parallel^{(I)}\beta|\ \delta H, \tag{4.69}$$

as shown in Fig. 4.14. Here the actual rates of change $(\delta\nu_n/\delta H)$ are $+0{\cdot}13$ kHz/G for the $M = +1$ Endor transitions, and $-0{\cdot}65$ kHz/G when $M = -1$, showing that the first term in (4.69) is comparable with the second. The main change in $A_\parallel$ arises from the variation in the orbital contribution to the hyperfine field, which is linked to the residual unquenched orbital momentum ($g_\parallel = 2{\cdot}195$) and hence to the splitting parameter D through the spin-orbit coupling.

In some cases such as ions with half-filled shells the hyperfine interactions are mainly due to effects such as core-polarization and relativistic effects (cf. § 4.7) which may be expected to be substantially independent of the crystal field. Thus variations in the latter which affect the fine structure parameters will have no corresponding effect on the hyperfine parameters. However there may still be some inhomogeneous broadening of the Endor line because of the inhomogeneous width ΔH of the electron resonance line, since the Endor frequency is not independent of H. For axial symmetry and an arbitrary direction of **H** the width of the Endor line can be found by differentiation of eqn (4.5) with respect to H, which is inherent both in G_I (see eqn (3.55)) and in $G = g\beta H$. For the special case where **H** is along the symmetry axis such a differentiation gives

$$\delta(h\nu_n) = \left|-g_\parallel^{(I)}\beta\ \Delta H + \left(\frac{A_\perp^2}{2h\nu_e}\right)\{S(S+1) - M^2 + M(2m-1)\}\ \frac{\Delta H}{H}\right|. \tag{4.70}$$

This expression has a complicated dependence on M and m, but is often smallest for the $M = +\frac{1}{2} \leftrightarrow -\frac{1}{2}$ transition simply because ΔH for the electron resonance line is also normally smallest for this transition.

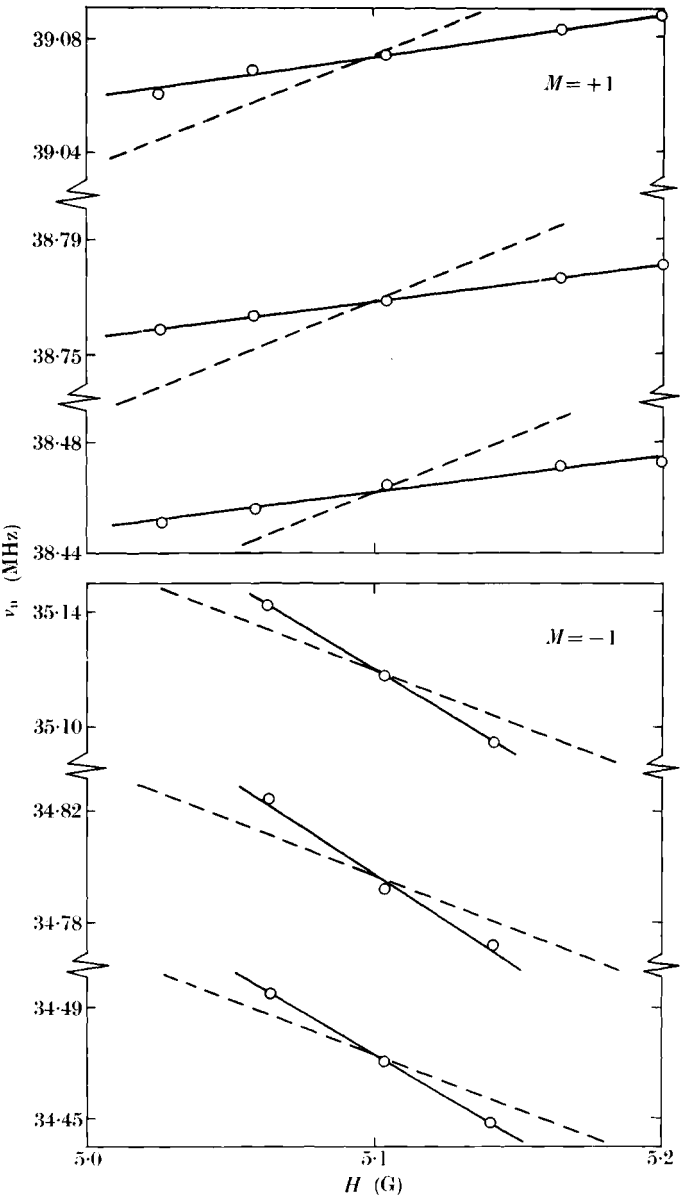

FIG. 4.14. The six Endor frequencies ν_n of ^{61}Ni observed in Al_2O_3 for $\mathbf{H} \parallel c$ axis at the $M = 0 \leftrightarrow +1$ e.p.r. line. H was varied within the broad e.p.r. line keeping the microwave frequency fixed. The points and the solid lines give the experimental results whereas the dashed lines indicate what would be expected if the hfs parameter, $A_{\parallel}$, were constant throughout the line. Note that the Endor transitions in the $M = -1$ states are also observed (though much more weakly than those in the $M = +1$ states) while saturating the $M = +1 \leftrightarrow 0$ transition (see § 4.11). (Locher and Geschwind 1963)

Since the effects discussed above depend on $g^{(I)}$ and on the magnetic hyperfine constant (either as A or A^2), and possibly also on the nuclear electric quadrupole parameter P, variation in these quantities will cause the inhomogeneous contribution to the Endor line width to vary from isotope to isotope of the same ion if the nuclear moments are different. There may also be a variation with m (cf. eqns (4.68) and (4.70)).

We conclude this discussion of inhomogeneous broadening of Endor lines by giving some numerical values. Locher and Geschwind (1963) deduced in their experiment on $^{61}Ni^{2+}$ in Al_2O_3 that on varying H by 200 G (going from A to C in Fig. 4.13) the variation in the hyperfine field H_e was some 130 G. Since the total orbital contribution to H_e is estimated as 170 kG, the change is fractionally very small though readily measurable; it corresponds to a frequency change of some 34 kHz whereas the half width at half intensity $2\delta\nu_n$ in the Endor lines was 23 kHz.

In contrast, the effect given by (4.70) can sometimes be quite small. In their experiments on Eu^{2+} Endor in CaF_2 (§ 4.7), Baker and Williams (1962) found line widths of 7 and 8 kHz respectively for the isotopes ^{153}Eu and ^{151}Eu, whose nuclear moments are in the ratio 1:2·27. In addition, the outer electron resonance lines gave the same Endor width as the $M = +\frac{1}{2} \leftrightarrow -\frac{1}{2}$ transition. These two facts indicate that inhomogeneous broadening of the Endor lines in this case was only very minor. We note also from (4.70) that the second term varies as ν_e^{-2} or H^{-2}, and its effect can be reduced by working at a higher electron resonance frequency. Thus Bessent and Hayes (1965) found for $^{169}Tm^{2+}$ in CaF_2 that the Endor width was reduced from 500 to 75 kHz on increasing the electron resonance frequency from 10 to 24 GHz. The second term in (4.70) is more important in this case because of the high value of $A = 1100$ MHz (isotropic), and the observed Endor widths correspond to $\Delta H \sim 30$ G, which is roughly the extent of the fluorine ligand hyperfine structure in the electron resonance line rather than the width of individual lines.

Cross-relaxation within the electron spin system

Cross-relaxation is due to the possibility of two nearby ions, some of whose resonance frequencies coincide, exchanging a quantum of energy and undergoing a 'flip-flop' transition. If one ion is subjected to an electron resonance driving field tending to equalize the populations of two specific levels, while the other belongs to another spin-packet which is

not at resonance, the effect of cross-relaxation is partially to transfer saturation to the second ion. Conversely, if a nuclear driving field tends to diminish saturation (or merely change populations of levels) in this second ion, the effect will also be felt by the first ion, and will be manifested as an Endor signal for the first ion.

As a specific example we refer to Fig. 1.34, where the $\Delta M = \pm 1$, $m = +1$ hyperfine line is saturated in a system $S = \frac{1}{2}$, $I = 1$. Normally we would expect to observe at most the $m = +1 \leftrightarrow 0$ nuclear transitions in such an Endor experiment. However, if the ions can make a spin flip corresponding to the left-hand sloping transition

$$(-\tfrac{1}{2}, +1) \leftrightarrow (+\tfrac{1}{2}, 0)$$

with other ions not undergoing saturation, both the $m = +1$ level populations for the first set of ions and the $m = 0$ populations for the second set will be changed. As a result, nuclear power applied to the $m = 0$ to -1 transitions on the second set of ions may appear as an Endor transition while saturating the $m = +1$ line of the first set.

The chance of such a cross-relaxation process occurring is greatly increased if the concentration of paramagnetic ions is raised. In an Endor experiment on $^{59}Co^{2+}$ ($I = \frac{7}{2}$, $S = \frac{1}{2}$) in MgO, Fry and Llewellyn (1962) found that at a concentration of 0·1 per cent Co they observed just $16IS = 28$ strong Endor transitions by saturating in turn each of the eight hyperfine lines. However at 0·5 per cent concentration the total number of Endor lines was close to 100; as a specific example, all fourteen Endor transitions $M = \pm\frac{1}{2}$, $\Delta m = \pm 1$ were observed (with varying intensity) while saturating the $(+\frac{1}{2}, -\frac{7}{2}) \leftrightarrow (-\frac{1}{2}, -\frac{7}{2})$ electron resonance line. The higher concentration not only makes cross-relaxation more likely because on average the paramagnetic ions are closer, but also because the greater line width makes it easier to satisfy the conditions for mutual spin flips, which may involve any allowed transition and not just the type quoted above. Obviously the greater line width is not purely inhomogeneous in nature, and results in a decrease in the value of τ_2 and an increase in the spin-packet width, giving greater Endor line widths.

Cross-relaxation in the nuclear spin system

In addition to mutual spin flips involving electronic transitions we may have spin flips involving nuclear transitions. The rate at which these occur depends on the size of the spin-spin interaction between nuclei and is thus obviously very much smaller than in the electronic case. This is particularly true for the central nuclei of the paramagnetic

ions themselves as they are comparatively far apart in a dilute crystal. On the other hand, when a ligand hyperfine structure is present, we are usually concerned with a number of nuclei of the same species separated by distances $\approx$ a few nm. For example, in CaF_2 the F^- ions lie on a simple cubic lattice of spacing 0·27 nm, and each Ca^{2+} is surrounded by a cube of eight F^- ions at a distance of 0·235 nm. When all F^- ions are equivalent, as in pure CaF_2, the spin-spin interaction between them gives an r.m.s. line width $2\delta\nu_n$ for the ^{19}F nuclear magnetic resonance varying from 12 to 29 kHz with the orientation of the external magnetic field (Van Vleck (1948), Pake and Purcell (1948)), which is partly due to mutual spin flip processes. We may therefore expect a line width of this order in the fluorine ligand Endor experiments discussed in § 4.9. When **H** is along a $\langle 110 \rangle$ direction, the value of $2\delta\nu_n$ is 20 kHz in the n.m.r. experiment, and Bessent and Hayes (1965) find a line width of 20 ± 12 kHz in the F^- endor in Tm^{2+}:CaF_2.

Although the n.m.r. line width should be equal to the Endor line width for more distant fluorine ions, whose immediate environment is similar to that in pure CaF_2, this is not necessarily the case for Endor of the F^- ions immediately adjacent to a paramagnetic ion. There are two reasons for this:

(a) such F^- ions experience a large local field from the paramagnetic ion, which even for a purely dipolar interaction is of order $\mu/r^3 = 10^3$ G if $S = \frac{1}{2}$, $g = 2$ and may be considerably larger. Hence the total field at these F^- nuclei differs considerably from that at more distant nuclei, thus eliminating the possibility of mutual spin flips except between the smaller number of nuclei in identical fields. This should give a smaller Endor line width for the immediate ligand nuclei of the paramagnetic ion:

(b) such F^- nuclear dipoles can, however, interact with one another indirectly via the paramagnetic ion, since terms of the form

$$\frac{\langle M, m^i | A_F S_+ I^i_- | M-1, m^i+1 \rangle \langle M-1, m^j+1 | A_F S_- I^j_+ | M, m^j \rangle}{h\nu_e} \tag{4.71}$$

and similar terms give an $(\mathbf{I}^i \cdot \mathbf{I}^j)$ interaction of order $A_F^2/(h\nu_e)$. If $A_F \sim 10$ MHz, $\nu_e = 10$ GHz, this interaction constant is of order 10 kHz, and may be multiplied by an appreciable numerical factor for larger values of S (e.g., $S = \frac{7}{2}$ for Eu^{2+}). This indirect interaction will increase the Endor line width, accounting for the observed value $\sim$40 kHz for F^- in Eu^{2+}:CaF_2 (Baker and Hurrell (1963)). For a fuller

discussion of the effects of such interactions, reference should be made to this paper.

4.11. 'Indirect' observation of Endor transitions

For an ion with $S = \frac{1}{2}$ the populations of the two electronic levels are both immediately affected by saturating an electronic transition. For $S \geqslant 1$, we have three or more electronic levels but the microwave power directly affects only two levels unless the resonance frequencies for several transitions coincide accidentally. Nevertheless relaxation proceeds between all the levels of a single ion at a rate $\sim 1/\tau_1$, so that the populations of all levels are indirectly affected by the saturating power after a time of order τ_1. This is illustrated in Fig. 4.15 for $S = 1$,

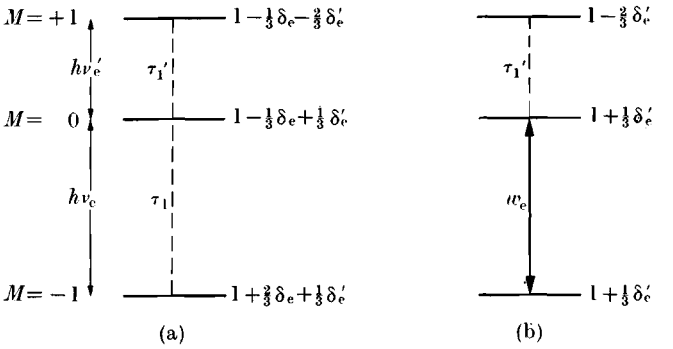

FIG. 4.15. Level populations within an electron spin system $S = 1$. (a) Levels in thermal equilibrium, with thermal populations according to their unequal spacing $\delta_e = (h\nu_e/kT)$, $\delta_e = (h\nu'_e/kT)$. (b) Populations when the lower transition $h\nu_e$ is saturated, showing how the population of the top level is also changed following relaxation through the path labelled τ'_1.

where there are two allowed transitions at different frequencies ν_e and ν'_e. If the $M = 0 \leftrightarrow -1$ transition for one hyperfine line $I_z = m$ is saturated, the population of the $M = +1$, m state is altered through a τ_1 relaxation path, while those of the other $M = +1$ nuclear levels depend on other relaxation paths that are usually less effective. It follows conversely that nuclear power applied to nuclear transitions within the $M = +1$ level can change the populations of the $M = 0$, -1 levels and may thus give an Endor signal while the $M = 0 \leftrightarrow -1$ transition is observed. The lower three Endor transitions in Fig. 4.14 were detected 'indirectly' in this way; they belong to the $M = -1$ electronic state but are observed through the electronic

$M = +1 \leftrightarrow 0$ transition. This is a result of population adjustments within the levels of a single paramagnetic ion resulting from spin-lattice relaxation processes.

We have already mentioned in § 4.10 how cross-relaxation processes due to spin-spin interactions in the electron spin system may allow Endor transitions to be observed indirectly for ions with $S = \frac{1}{2}$, and such effects are equally possible for ions with $S \geqslant 1$. We now discuss similar effects arising from cross-relaxation within a nuclear spin system.

If we have a system of identical spins in which the level populations at one point in the specimen differ from those at other points, the spin flip process will act to make the population differences uniform throughout the specimen. This process is known as 'spin diffusion'; essentially it creates a uniform 'spin temperature' throughout the specimen, and without it the concept of a 'spin temperature' would be thermodynamically meaningless, or at least trivial as in the case of a single spin. It is particularly important in methods of dynamic nuclear polarization (cf. § 1.12) for ligand nuclei. If the ligand nuclei in the neighbourhood of a paramagnetic ion become polarized through interaction with this ion while a strong microwave field near its electron resonance frequency is being applied, the polarization is gradually transferred to more distant nuclei through spin diffusion. (There is of course a barrier to this for the closest ligand nuclei, because they experience different local fields due to their proximity to the paramagnetic ion and are thus not at the same resonance frequency as more distant ligand nuclei.) The process of polarizing more distant nuclei involves a flow of energy, whose ultimate source must be the electron resonance oscillatory field, through the paramagnetic ion. The electron resonance intensity of the latter can therefore be sensitive to population differences on quite distant nuclei (of which there are many), giving the possibility of an Endor experiment on such nuclei. Clearly this type of 'distant Endor' process is closely linked with that of dynamic nuclear polarization, as might be expected from similarities in the treatment of §§ 1.12 and 1.13. It is also linked with the fact that the principal agents in relaxing nuclear spins in a solid are very commonly paramagnetic ions, which are in very much more intimate contact with the lattice than the nuclear spin system.

A study of 'distant Endor' has been made for the system $Cr^{3+}:Al_2O_3$ (ruby) by Lambe, Laurance, McIrvine, and Terhune (1961). Essentially they found that

(a) the behaviour of the electron resonance signal is complicated; when nuclear power is applied to the ^{27}Al ($I = \frac{5}{2}$) system, the dispersion signal (χ') is decreased at points away from the centre of the electron resonance line, while the absorption signal (χ'') is increased at such points;

(b) such effects are observed when the nuclear frequency was that required for nuclear resonance on Al nuclei which are so far away that their nuclear resonance frequency is not shifted through interaction with the magnetic field of the Cr^{3+} ion;

(c) the recovery time of the electron resonance signal after removal of the nuclear power was comparable with the nuclear spin-lattice relaxation time ($\sim$10 s), whereas the Endor mechanisms discussed in §§ 4.5 and 4.6 would lead to a recovery time of order of the electronic spin-lattice relaxation time $\tau_1 \sim 0{\cdot}1$ s.

The authors concluded that the distant Al nuclei were being polarized by the $S^{\pm}I^{\pm}$, $S^{\pm}I^{\mp}$ terms in their interaction with the paramagnetic ions (the mechanism discussed at the end of § 1.12), which are effective when the electron resonance frequency is on either side of its central frequency. Depolarization of the Al nuclei occurs when nuclear magnetic resonance power is applied to them, and conversely this affects the electron resonance signal in the wings, not in the centre, at the points where the electron resonance frequency has the required value to produce dynamic nuclear polarization (cf. Fig. 1.39).

4.12. Summary

We conclude the discussion of Endor by recapitulating some of the salient features of this type of experiment.

(a) *High sensitivity.* Nuclear magnetic resonance transitions are observed through their effect on the electron paramagnetic resonance signal, in many cases aided by the considerable enhancement of the nuclear transition probability brought about through 'stirring' of the hyperfine field by the nuclear oscillatory field.

(b) *Direct measurement of hyperfine frequencies with high accuracy.* For inhomogeneously broadened electron spin resonance lines, Endor line widths lie in the region 10–50 kHz, so that Endor frequencies even of order 10^3 MHz can be measured to a few kHz. This makes it possible to observe high-order effects in the hyperfine structure of the paramagnetic ion with its own nucleus, as well as ligand hyperfine structure associated with electron transfer and bonding with ligand ions. However in solids the nuclear Zeeman interaction can be drastically changed

by the 'pseudo-nuclear Zeeman effect'; thus g_I is often not determined as accurately as is possible using triple resonance methods in atomic beam measurements on free atoms, where the corrections are smaller and can be calculated more accurately.

(c) *At least three mechanisms for the Endor process are possible—'packet shifting'* (§ 4.4), *change in rate of relaxation to lattice* (§ 4.6), *and 'distant Endor'* (§ 4.10).